AUTHOR QUERY FORM

Dear Author,

During the preparation of your manuscript for publication, the questions listed below have arisen. Please attend to these matters and return this form with your proof.

Many thanks for your assistance.

Query References	Query	Remarks
1	Author please confirm suggested keywords	

R

7
Membrane Electroporation in High Electric Fields

Rumiana Dimova

7.1
Introduction

The autonomy of a cell, the basic building unit of most living creatures, is ensured by a bounding membrane. The scaffold of this membrane is made of a double lipid layer, which is basically impermeable to all substances in the cellular environment except for water. The mechanical and rheological properties of the bilayer define the response of the membrane to external perturbations. The membrane "intolerance" towards letting solute molecules easily cross it creates the main obstacle in biomedical applications where drugs or genes have to be introduced into cells. One approach finding broad use nowadays in overcoming the barrier functions of membranes relies on the temporary bilayer perforation when exposed to strong electric fields. This phenomenon, called electroporation, is the main focus of this chapter.

The main topics to be covered build upon our knowledge of the mechanical and rheological properties of membranes and their response to perturbations. In the remaining parts of this introductory section, some of these properties are briefly described to set the basis for a discussion of the behavior and response of membranes to external forces. The following sections consider in detail the morphological changes and poration electric fields can induce in vesicles made of membranes in different phases, and the effects of media environment and various molecular inclusions in the lipid bilayer, that is, the specific membrane composition. Finally, some application aspects of the work are discussed.

7.1.1
Giant Vesicles as Model Membrane Systems

The field of membrane structure and characterization is attracting the attention of a growing number of researchers. The basic research in this area builds upon studies performed on the simplest and minimal systems mimicking cell membranes, namely model membranes. Examples of such model membranes are

Advances in Electrochemical Science and Engineering. Edited by Richard C. Alkire, Dieter M. Kolb, and Jacek Lipkowski

ISBN: 978-3-527-32885-7

lipid monolayers at the air–water interface, solid-supported bilayers, black lipid membranes, vesicles, and bilayer stacks. Among them, vesicles or liposomes are membrane "bubbles" formed by bending and closing up of a lipid bilayer. They are the most natural systems, because, in terms of shape and structure, they are closest to membranes of cells and cell organelles.

Various experimental techniques have been developed for preparing liposomes of different sizes (from nanometers to tens of micrometers) [1]. The largest ones, several tens of micrometers in size, are called "giant vesicles" [2] and are an extraordinarily convenient system for studying membrane behavior [3, 4]. They are well visible under an optical microscope using various enhancing techniques like phase contrast, differential interference contrast, or confocal and conventional fluorescence microscopy, the latter two being particularly useful in distinguishing domains on membranes (Figure 7.1). Thus, giant vesicles allow for direct manipulation and observation of membrane interactions and responses to external perturbations. On the contrary, working with conventional vesicles (a few hundreds of nanometers) usually involves the application of indirect methods and techniques for observation. In addition, their small sizes often raise questions about effects due to high membrane curvature when molecular interactions are considered. In contrast, giant vesicles, which have sizes in the micrometer range (i.e., comparable to the sizes of cells), and therefore have nearly zero membrane curvature, reflect the properties and behavior of cell plasma membranes.

Colour Figure

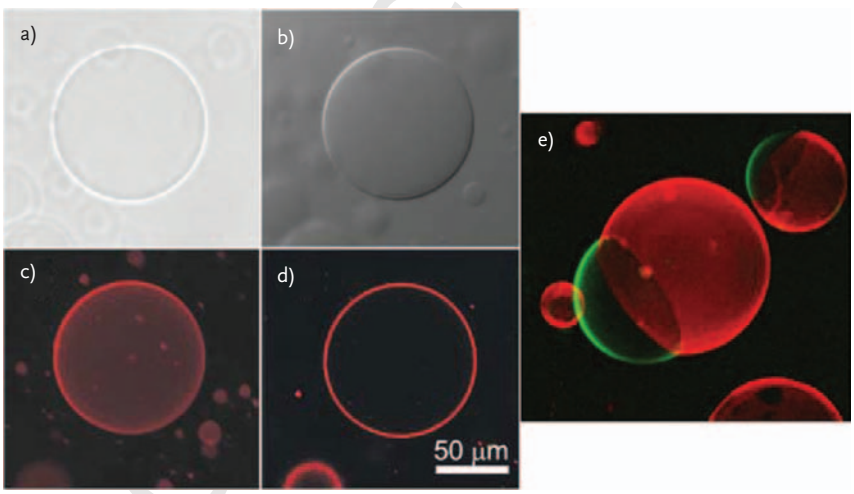

Figure 7.1 Snapshots of the same giant vesicles observed under different microscopy modes: (a) phase contrast; (b) differential interference contrast; (c) projection averaged confocal microscopy; (d) equatorial section confocal microscopy. Adapted from [3] by permission of IOP Publishing Ltd. (e) Confocal three-dimensional projection image of vesicles with immiscible fluid domains visualized with fluorescent dyes, which preferentially partition in one or the other lipid phase.

The two most popular techniques for the formation of giant vesicles (other available methods are summarized in [4]) are spontaneous swelling or gentle hydration, introduced by Reeves and Dowben [5] and electroswelling, introduced by Angelova and Dimitrov [6]; for a brief description of these two preparation protocols, see [3]. These two methods were further developed and improved by several groups (e.g., [4, 7–10]). Interestingly enough, the underlying mechanism of the electroformation protocol, which is based on exposing lipid layers to alternating electric fields, is still poorly understood even though widely used. Both protocols yield giant vesicles with sizes in the range of a few tens of micrometers.

Giant unilamellar vesicles (GUVs) are increasingly employed for quantitative characterization of the physicochemical properties of lipid membranes with various compositions, but also to study membrane-related processes like cell adhesion, phase separation and domain formation, protein sorting in lipid rafts, endo- and exocytosis, uptake of various molecules, and protein mobility, to mention just a few of the studied fields. Examples of using GUVs as simple model systems for unraveling certain physicochemical properties of biological membranes include lipid domain formation [11–13], mechanical and rheological properties of the entire vesicle [14] or of the membrane [3, 15, 16], lipid dynamics, membrane growth [17–20], membrane adhesion [21–25], wetting phenomena [26, 27], budding and fission [28–32], and membrane fusion [33–37]. Giant vesicles are also a very practical tool to study the response of membranes to external perturbations like hydrodynamic flows [38], locally applied forces [39], micromanipulation [40], and electric fields [41, 42]. This chapter focuses on the effects of strong electric pulses on model membranes as exhibited by the behavior of GUVs exposed to such pulses. The vesicle response will be interpreted in view of general concepts of membrane biophysics.

7.1.2 Mechanical and Rheological Properties of Lipid Bilayers

The physical properties of lipid bilayers are those that define their response to external perturbations. Knowing the mechanical and rheological characteristics of lipid membranes will prepare us to tackle problems related to stress induced in bilayers by electric fields and the phenomena that it triggers, for example, dynamics of vesicle and cell deformation, bilayer instability, electroporation, and electrofusion.

As a simple depiction of a lipid bilayer, one can consider it as a film or a slab, which may be curved, compressed or dilated, and sheared. At physiological temperatures most natural lipid membranes are fluid. Therefore, within this slab, the lipid molecules are free to move. Below the lipid phase transition temperature, single-component membranes crystallize. In this so called "gel" phase, the relative motion of lipids and membrane inclusions is principally hindered. The fluidity of the membrane and resistance to shear in the plane of the film are characterized by the shear viscosity, η_s (or the diffusion coefficient of the lipids). Typical values

of η_S lie in the range 1×10^{-9}–5×10^{-9} N s m^{-1} [16] for fluid membranes, but for gel-phase membranes divergence is observed [43]. One may equivalently define a viscosity η_D related to the dilation and compression of the membrane. The value of η_D is of the order of 3.5×10^{-7} N s m^{-1} [44].

Phospholipid membranes in the fluid phase are very soft: the energy required for their bending is comparable to the thermal energy. The bilayer bending rigidity, κ, which characterizes how easy it is to curve the lipid bilayer, is typically of the order of 0.9×10^{-19} J, which is equivalent to $20k_BT$ [45–47], where k_B is the Boltzmann constant and T is the absolute temperature. Thus, fluid membranes fluctuate due to thermal noise. These fluctuations can be directly observed on tensionless giant vesicles under the microscope, which is the basis of the so-called fluctuation spectroscopy method used to measure membrane bending rigidity [48–55]. For gel-phase membranes, the bending rigidity increases significantly, and a few degrees below the main phase transition temperature it reaches values of the order of $(15–20) \times 10^{-19}$ J (about $350k_BT$) [43, 56, 57].

Weak tensions applied to a fluid membrane smooth out bilayer undulations. At high tensions the membrane can be stretched leading to a change in the area per lipid molecule. The stretching elasticity modulus, K_a, characterizing this response is of the order of that of a rubber sheet with the same thickness (about 4 nm). Typical values of K_a for fluid membranes lie in the range 200–300 mN m^{-1} [47] and for gel-phase membranes can reach values of 850 mN m^{-1} [58]. Upon stretching, a lipid bilayer can sustain tensions up to several mN m^{-1}. At a certain critical tension, also known as the lysis tension, σ_{lys}, the membrane ruptures. For fluid membranes, σ_{lys} is of the order of 5–10 mN m^{-1} [59, 60]. Note that the membrane tensile strength depends on the tension loading rate [61]. Membranes in the gel phase can sustain higher tensions and rupture at higher values of σ_{lys} [62].

After rupture or poration, the rearrangement of the lipids to close the bilayer sheet is energetically favorable because in this way the hydrophobic tails of the lipid molecules are shielded from exposure to water. The energy penalty of closing a hole in the membrane is described by the edge tension, γ, which is of the order of several piconewtons [63]. The edge tension plays a strong role in processes of pore stability and resealing as in electroporation, which is discussed in more detail in Section 7.5.1.

7.2
Electrodeformation and Electroporation of Membranes in the Fluid Phase

Vesicles exposed to electric fields deform. The response of GUVs to electric fields has been the subject of extensive investigation. When exposed to AC electric fields, as a stationary state they attain ellipsoidal shapes – prolate or oblate – depending on the field frequency and media conductivity [42, 64]. Initiated by the seminal work of Winterhalter and Helfrich [65], this effect has been considered theoretically [66–74] and experimentally [42, 64, 67, 75–77], whereby interesting dynamics and flows in the membrane and in the surrounding medium were observed

[78, 79]. This chapter mainly discusses the response of giant vesicles to short DC rectangular pulses with duration in the range 100 μs–5 ms. Parallels to the vesicle behavior in AC fields will be also drawn. In this section, only vesicles in the fluid phase will be considered. In Section 7.3, we will discuss the response of vesicles in the gel phase and compare it to that of fluid vesicles.

While vesicle deformation in AC fields concerns stationary shapes, DC pulses induce short-lived shape deformations. In different studies, the pulse duration has been typically varied from several microseconds to milliseconds, while studies on cells have investigated a much wider range of pulse durations – from tens of nanoseconds to milliseconds and even seconds [80], as discussed in other chapters of this book. Various pulse profiles, unipolar or bipolar, as well as trains of pulses have been also employed (e.g., [81, 82]). Because the application of both AC fields and DC pulses creates a transmembrane potential, vesicle deformations of similar nature are to be expected in both cases. However, the working field strength for DC pulses is usually higher by several orders of magnitude. Thus, the degree of deformation can be different.

Vesicle deformation induced by DC pulses has been studied theoretically [83–85]. The majority of experimental studies were preformed on small vesicles of hundreds of nanometers in size [86–88], but their size did not allow for direct observation of the deformation dynamics. Employing fast digital imaging, recently we succeeded in revealing vesicle deformation [89], whereby the vesicle response was recorded with high temporal resolution of up to 30 000 frames per second (fps), that is, acquiring an image every 33 μs. The GUVs were observed to deform into a prolate ellipsoid during the pulse and subsequently relax back to their initial spherical shape.

The degree of deformation of an ellipsoidal vesicle can be characterized by the aspect ratio of the two principal radii, a and b (see the inset of Figure 7.2). For $a/b = 1$ the vesicle is a sphere. In the absence of poration, that is, relatively weak or short pulses, the relaxation can be described by a single exponential with a characteristic decay time, τ_1. Figure 7.2 gives one example of the response of a giant vesicle, which is initially spherical. The maximum deformation of this vesicle corresponds to an about 10% change in the vesicle aspect ratio. The degree of vesicle deformation depends on the initial tension of the vesicle as well as on the excess area [90], the latter being defined as an excess compared to the area of a spherical vesicle with identical volume.

The typical decay time for the relaxation of nonporated vesicles, τ_1, is of the order of 100 μs. It is set by the relaxation of the membrane tension achieved at the end of the pulse. The membrane tension, σ_{el}, acquired during the pulse, also referred to as "electric tension," arises from the transmembrane potential, Ψ_m, built across the membrane during the pulse. Lipid membranes are impermeable to ions and, in the presence of an electric field, charges accumulate on both sides of the bilayer, which gives rise to this transmembrane potential [91]:

$$\Psi_m(t) = 1.5R|\cos\theta|E\left[1-\exp\left(\frac{-t}{t_c}\right)\right] \tag{7.1}$$

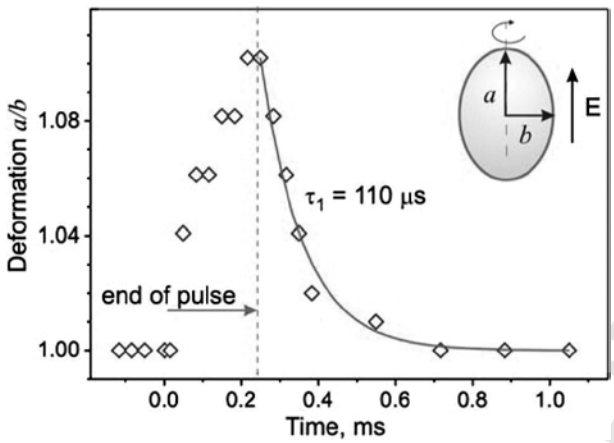

Figure 7.2 Time dependence of the degree of deformation, a/b, of a vesicle exposed to a square-wave DC pulse with field strength $E = 100\,\mathrm{kV\,m^{-1}}$ and pulse duration $t_p = 250\,\mu\mathrm{s}$. The solid curve is an exponential fit with a decay time τ_1 as indicated. The inset schematically illustrates the shape of the deformed vesicle and the principal radii. The dashed line indicates the end of the pulse. Adapted from [89] by permission of the Biophysical Society.

where R is the radius of a spherical vesicle, θ is the tilt angle between the electric field and the surface normal, t is time, and t_c is the charging time as defined by

$$t_c = RC_m\left(\frac{1}{\lambda_{in}} + \frac{1}{\lambda_{ex}}\right) \tag{7.2}$$

Here, λ_{in} and λ_{ex} are the conductivities of the solutions inside and outside the vesicle, respectively. Equations (7.1) and (7.2) are valid only for a nonconductive membrane.

The effective electrical tension, σ_{el}, induced by the transmembrane potential, Ψ_m, is defined by the Maxwell stress tensor [59, 89, 92]

$$\sigma_{el} = \varepsilon_m\left(\frac{h}{2h_e^2}\right)\Psi_m^2 \tag{7.3}$$

Here h is the total bilayer thickness (≈4 nm), h_e is the dielectric thickness (≈2.8 nm for lecithin bilayers [93, 94]), and ε_m is the membrane permittivity ($\approx 2\varepsilon_0$, where ε_0 is the vacuum permittivity). For vesicles with some initial tension σ_0, the total tension reached during the pulse is simply

$$\sigma = \sigma_0 + \sigma_{el} \tag{7.4}$$

As mentioned above, the decay time for the relaxation of nonporated vesicles, τ_1, is defined by the total membrane tension at the end of the pulse. The tension relaxation requires relative displacement of the lipid molecules in the bilayer,

whose intermolecular distance is increased during the pulse, that is, the membrane is stretched. This relative displacement is characterized by the dilational viscosity η_D as introduced in Section 7.1.2. Thus, τ_1 relates mainly to the relaxation of membrane stretching: $\tau_1 \sim \eta_D/\sigma$. For membrane tensions of the order of $5\,\mathrm{mN\,m^{-1}}$ (which should be around the maximum tension before the membrane ruptures, $\sigma \approx \sigma_{lys}$) and for typical values of η_D, one obtains $\tau_1 \sim 100\,\mu s$, which corresponds to the experimentally measured value (see Figure 7.2).

Above some electroporation threshold, the transmembrane potential Ψ_m cannot be further increased, and can even decrease due to transport of ions across the membrane [91, 95]. The phenomenon of membrane electroporation can also be understood in terms of tension. If the total membrane tension exceeds the lysis tension σ_{lys}, the vesicle ruptures. This corresponds to building up a certain critical transmembrane potential, $\Psi_m = \Psi_c$. According to Eqs. (7.3) and (7.4), this poration potential Ψ_c depends on the initial membrane tension σ_0 as previously reported [59, 89, 90, 96, 97]. The critical transmembrane potential for cell membranes is about 1 V (e.g., [98, 99]).

Vesicle poration induced by DC pulses has been studied extensively, initially mainly on small vesicles [88, 100, 101]. Experiments on giant vesicles are of special relevance because their size allows for direct observation using optical microscopy [37, 89, 102–107]. The pores can reach various sizes depending on the location on the vesicle or cell surface (e.g., [99, 108] and work cited therein). For the case of plane parallel electrodes, the poration occurs predominantly in the area at the poles of the vesicle facing the electrodes. This is because the transmembrane potential attains its maximal value at the two poles as expressed by the angular dependence in Eq. (7.1). With optical microscopy, only pores that are of diameter larger than about 0.5 μm can be resolved. We refer to them as macropores. The lifetime of macropores, τ_{pore}, observed in vesicles in the fluid state, varies with pore radius, r_{pore} [104], and depends on the membrane edge tension, γ, and the membrane dilatational viscosity: $\tau_{pore} \approx 2r_{pore}\eta_D/\gamma$. For phosphatidylcholine vesicles with low tension, the lifetime τ_{pore} is typically shorter than 30 ms [89]. The effect of membrane edge tension on pore resealing is discussed in detail in Section 7.5.1.

Figure 7.3a shows the time dependence of the deformation of vesicles in which macropores were observed. The maximum deformation is much higher than that observed for nonporated vesicles (compare with the aspect ratio a/b in Figure 7.2). The typical relaxation time is $\tau_2 \approx 7 \pm 3$ ms. The relaxation process associated with τ_2 takes place during the time interval when pores are present (shaded region in Figure 7.3a; snapshots of a porated vesicle are shown in Figure 7.3b). Thus, τ_2 is determined by the closing of the pores: $\tau_2 \approx \eta_D r_{pore}/2\gamma$. The edge tension $\gamma$is of the order of 10^{-11} N [109, 110]. For a typical pore radius of 1 μm one obtains $\tau_2 \approx 10$ ms. When the vesicles have some excess area, the relaxation proceeds in two steps: a fast relaxation characterized by τ_2 and a second, longer, relaxation with decay time τ_3: $0.5\,s < \tau_3 < 3\,s$ [89]. This relaxation time is related to the presence of some excess area available for shape changes corresponding well to the experimentally measured value.

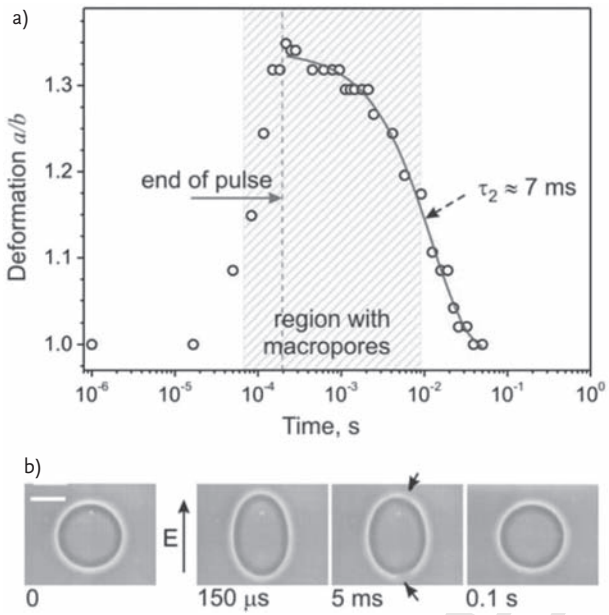

Figure 7.3 Deformation of macroporated phosphatidylcholine vesicles exposed to rectangular DC pulses with amplitude $E = 200\,\mathrm{kV\,m^{-1}}$, and pulse duration $t_p = 200\,\mu\mathrm{s}$. (a) Time dependence of the degree of deformation a/b of a vesicle. Time $t = 0$ was set as the beginning of the pulse. The dashed line indicates the end of the pulse. The relaxation of the vesicle is described by a single exponential fit (solid curve) with a decay time τ_2 as indicated. The shaded area indicates the time interval when macropores were optically detected. (b) Snapshots from another vesicle before, during, and after poration. The time after the beginning of the pulse is indicated below each micrograph. The scale bar corresponds to 15 µm. The arrows in the third image point to the porated zones, which are visualized as interruptions in the bright halo around the vesicle. Adapted from [89] by permission of the Biophysical Society.

7.3 Response of Gel-Phase Membranes

As discussed in Section 7.1.2, the mechanical and rheological properties of membranes in the gel phase differ significantly from those of fluid membranes. These differences introduce new features in the response of gel-phase membranes to electric fields. We compared the response to DC pulses of a vesicle in the fluid phase with that of a vesicle in the gel phase. The applied DC pulses were weak enough not to induce formation of macropores in the membranes. Figure 7.4a shows the deformation of the two vesicle types in response to DC pulses with duration of 300 µs. To achieve similar maximal degree of deformation in vesicles with comparable radii, stronger pulses have to be applied to the gel-phase vesicle as compared to the fluid one. Pulses with field strength of about $100\,\mathrm{kV\,m^{-1}}$ do not produce optically detectable deformations in gel-phase vesicles, while strong

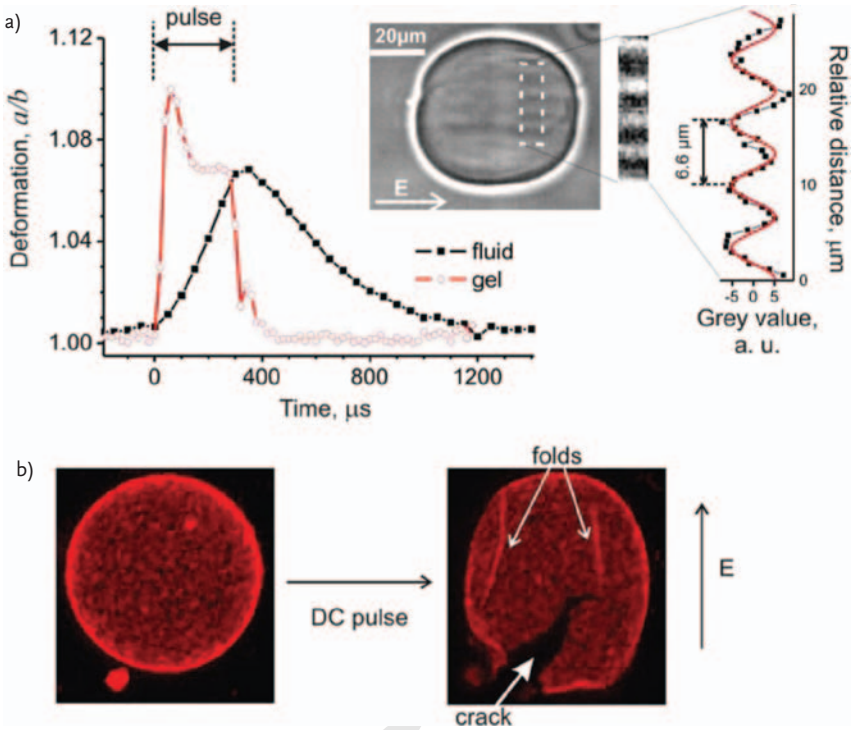

Colour Figure

Figure 7.4 Deformation and electroporation of gel-phase vesicles. (a) Deformation response of a gel-phase vesicle with a radius of 22 µm, and a fluid-phase vesicle with a radius of 20 µm. The applied rectangular DC pulses were of duration of 300 µs as indicated. The field strength of the pulses was 500 and 80 kV m^{-1} for the gel and the fluid vesicle, respectively, which is below the corresponding poration thresholds for the two types of membranes. The gel-phase vesicle exhibits an intrapulse relaxation arising from wrinkling of the membrane. The vesicle wrinkling is visible in the inset snapshot recorded at time t = 200 µs. A magnified and enhanced section of the image indicated with a dashed rectangle is given to the right of the image, showing the membrane wrinkling parallel to the electric field direction. The gray value intensity from such a section is plotted and fitted with a sinusoidal function. The corresponding wavelength of the wrinkles is about 6.6 µm as indicated. (b) Electroporation of a gel-phase vesicle with radius 25 µm observed with confocal microscopy. Before the pulse, the vesicle has a spherical shape. After applying a pulse with field strength of 600 kV m^{-1} and duration of 300 µs, the vesicle cracks open and folds as indicated by the white arrows. The field direction is indicated with a vertical arrow. The second image was recorded a few seconds after the end of the pulse. A relatively large crack is visible in the vesicle as shown in the three-dimensional projection of the vesicle top part. Adapted from [111] by permission of the Royal Society of Chemistry.

pulses of about 500 kV m^{-1} applied to fluid-phase vesicles cause poration. The fluid vesicle gradually deforms and reaches maximal deformation (maximal aspect ratio a/b) at the end of the pulse as in Figure 7.1. The gel-phase vesicle responds significantly faster, and exhibits a relaxation with a decay time of about 50 µs already during the pulse. This unusual intrapulse relaxation was found to be due to wrinkling of the membrane [111] as shown with the inset in Figure 7.4a. Typical wavelengths of the wrinkles, Λ, lie in the range 5–8 µm and were found to obey laws for wrinkling of elastic sheets [112–114]: $\Lambda = 2(\pi^2 L^2 \kappa/\sigma)^{1/4}$, where L is the characteristic length of the system, which in our case is the vesicle size, $L \approx 2R$. The bending stiffness, κ, of membranes in the gel phase is orders of magnitude greater than that of fluid membranes (see Section 7.1.2), which is one of the reasons why wrinkling of fluid vesicles is not observed. Furthermore, fluid membranes have zero shear modulus and deform smoothly rather than exhibiting wrinkles.

The behavior of gel-phase vesicles exposed to stronger pulses above the poration threshold is also significantly different from that of porated fluid membranes. While pores in GUVs made of lipids in the fluid phase reseal within a few tens of milliseconds (Section 7.2), gel-phase giant vesicles exhibit long-living pores [42, 111]. The pores may resemble cracks on solid shells (Figure 7.4b), which remain open for minutes. Similar arrest was reported for mechanically induced pores in membranes below the main phase transition temperature [58]. Having in mind that the pore lifetime is defined by the membrane viscosity ($\tau_{pore} \approx 2r_{pore}\eta_D/\gamma$, see Section 7.2), it is easy to understand the long lifetime of pores in gel-phase membranes. The membrane viscosity diverges when the membrane crosses the main phase transition [43]. Thus, the resealing process is strongly suppressed. The irregular shape of the pores in gel-phase vesicles may be further indicative of the relatively low edge tension in such membranes.

Above we discussed the behavior of macroporated giant vesicles. Electroporated gel-phase vesicles with sizes in the region of 100 nm were reported to reseal within milliseconds [100, 115]. For pores created in such vesicles, the pore radius, r_{pore}, should be in the nanometer range, yielding pore lifetimes, τ_{pore}, that are three orders of magnitude shorter than those of the micrometer-size pores in giant vesicles. Furthermore, the fields applied in [100, 115] were of the order of 30 kV cm^{-1}. Such pulses induce Joule heating resulting in a temperature increase of up to 15 K [115], which can bring the membranes close to and even above the pretransition temperature of the investigated lipid and lead to a decrease in the membrane viscosity. Finally, recent coarse-grain simulations on gel-phase vesicles with similar sizes suggest that below the main phase transition temperature a fraction of the lipids in such highly curved membranes remain in the fluid phase [116], which may further facilitate pore closure. To summarize, the response of small and giant vesicles in the gel phase to DC pulses above the poration threshold differs significantly.

One additional feature that differentiates the response of gel-phase from fluid-phase membranes is the critical poration threshold. As demonstrated in Figure 7.4a, pulses that porate fluid vesicles lead only to deformation of gel-phase GUVs.

The critical transmembrane potential for the latter was found to be in the range 8–10 V [111]. This value is significantly higher than the critical potential of 1 V reported for fluid membranes [59, 98, 99]. Thus, membranes in the gel phase can stand higher tensile stresses (see Eqs. (7.3) and (7.4)). This is also confirmed by micropipette aspiration experiments showing that fluid-phase dimyristoylphosphatidylcholine membranes undergo lysis at tensions around 2–3 mN m^{-1}, but when in the gel phase, the membranes rupture at tensions above 15 mN m^{-1} [62]. It is important to note that the rupture process depends on the loading rate [61, 117, 118]. At high loading rates a membrane can sustain much higher tensions before it ruptures. Similar behavior was demonstrated by simulation studies, where fluid dipalmitoylphosphatidylcholine (DPPC) bilayers were shown to spontaneously rupture at tensions exceeding 90 mN m^{-1} [119].

7.4
Effects of Membrane Inclusions and Media on the Response and Stability of Fluid Vesicles in Electric Fields

In the previous two sections we discussed the electrodeformation and electroporation of vesicles made of single-component membranes in water. In this section, we consider the effect of salt present in the solutions. The membrane response discussed above was based on data accumulated for vesicles made of phosphatidylcholines (PCs), the most abundant fraction of lipids in mammalian cells. PC membranes are neutral and predominantly located in the outer leaflet of the plasma membrane. The inner leaflet, as well as the bilayer of bacterial membranes, is rich in charged lipids. This raises the question as to whether the presence of such charged lipids would influence the vesicle behavior in electric fields. Cholesterol is also present at a large fraction in mammalian cell membranes. It is extensively involved in the dynamics and stability of raft-like domains in membranes [120]. In this section, apart from considering the response of vesicles in salt solutions, we introduce trends in the vesicle behavior of fluid-phase vesicles when two types of membrane inclusions are introduced, namely cholesterol and charged lipids.

7.4.1
Vesicles in Salt Solutions

In the presence of salt in a vesicle exterior, unusual shape changes are observed during an applied DC pulse [107]. The vesicles adopt spherocylindrical shapes (Figure 7.5) with lifetimes of the order of 1 ms. These deformations occur only in the presence of salt outside the vesicles, irrespective of their inner content (note that, in the absence of salt in the external solution, the vesicles deform only into prolates; see Figure 7.5a). When the solution conductivities inside and outside are identical, $\lambda_{in} \approx \lambda_{ex}$, vesicles with square cross section are observed (Figure 7.5d). For the case $\lambda_{in} < \lambda_{ex}$, the vesicles adopt disc-like shapes (Figure 7.5c), while in the

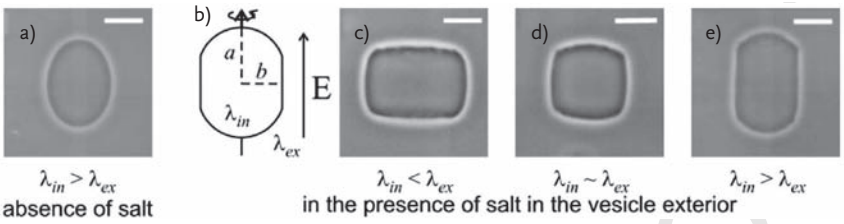

Figure 7.5 Deformation of vesicles in the absence and in the presence of salt at different conductivity conditions subjected to DC pulses (200 kV m^{-1}, 200 µs). (a) In the absence of salt in the external solution, prolate deformation is observed. (b) Schematic of a cross section of a vesicle, which has adopted spherocylindrical deformation (a cylinder with spherical caps) when salt is present in the vesicle exterior. The field direction is indicated with an arrow. The presence of salt flattens the vesicle walls into (c) disc-like, (d) "square"-like, and (e) tube-like shapes. The scale bars correspond to 15 µm. Adapted from [107] by permission of the Biophysicsl Society.

opposite case, $\lambda_{in} > \lambda_{ex}$, they deform into long cylinders with rounded caps (Figure 7.5e).

Analogy can be drawn between the cylindrical shapes observed in the presences of salt at various conductivity conditions and the elliptical morphologies of vesicles exposed to AC fields. The beginning of Section 2 briefly discussed the latter shapes. In AC fields, vesicles attain different deformations: prolate (with the long principal radius oriented in the field direction) and oblate (with the long principal radius oriented perpendicular to the field direction). For a fixed field frequency in the range 10^4–10^6 Hz, the type of deformation depends on the solution conductivities [42, 64]. In particular, vesicles with lower internal conductivity ($\lambda_{in} < \lambda_{ex}$) adopt oblate shapes ($a/b < 1$), analogously to the disc-like deformation in Figure 7.5c, whereas vesicles with higher internal conductivity ($\lambda_{in} > \lambda_{ex}$) adopt prolate shapes ($a/b > 1$), analogously to the tube-like deformation shown in Figure 7.5e. However, in AC fields, no flattening of the vesicles is observed.

The cylindrical deformations shown in Figure 7.5 are nonequilibrium shapes and have a very short lifetime, which is why they have not been observed previously when standard video acquisition speed was accessible only. The flattening of the vesicle walls starts during the applied pulse and is observed throughout a period of about 1 ms. So far, cylindrical deformations have not been observed in studies on cells [121, 122]. However, the temporal resolution in those experiments (3.3 ms per image) was not high enough to detect such short-lived deformations.

The formation of the spherocylindrical shapes is not well understood. They are observed not only on lipid vesicles but also on polymersomes (vesicles made of diblock copolymers [123, 124]) [107]. Therefore, lipid-specific effects, for example partial head group charge and membrane thickness, as a possible cause for the observed cylindrical deformations are to be excluded. One possible explanation could be that ions flatten the equatorial zone of the deformed vesicle. During the pulse there is an inhomogeneity in the membrane tension due to the fact that the

electric field is strongest at the poles of the vesicle, and almost zero close to the equator. The kinetic energy of the accelerated ions "hitting" the equatorial (tensionless) region of the vesicle is higher than the energy needed to bend the membrane, thus presumably leading to the observed deformation. To a certain extent, the effect of the ions could be considered as that of tiny particles subject to electrophoresis. Indeed, cylindrical deformations were observed also in quasi-salt-free solutions but in the presence of small negatively charged nanoparticles (40 nm in radius) in the vesicle exterior [42]. Thus, particle-driven flows may be yet another possible factor inducing membrane instability and giving rise to higher order modes of vesicle shape [125]. Another effect that could be considered is related to a local change in the spontaneous curvature of the bilayer due to the ion or particle asymmetry across the membrane [126]. During the pulse, local and transient accumulation of particles or ions in the membrane vicinity can occur inducing a change in the bilayer spontaneous curvature and driving the cylindrical deformations. Furthermore, another influencing factor might be an electrohydrodynamic instability caused by electric fields interacting with flat membranes, which was predicted to increase membrane roughness [127]. Finally, the flexoelectric properties of lipid membranes, first postulated by Petrov and coworkers [128–130], may also be involved as recently proposed [73, 131]. The interplay between surface ion concentration gradients combined with the overall ionic strength and bilayer material properties and tension could be expected to produce the observed cylindrical deformations.

7.4.2
Vesicles with Cholesterol-Doped Membranes

In order to understand the complex behavior of cellular membranes and their response to external perturbations like electric fields, one has to elucidate the basic mechanical properties of the lipid bilayer. The significant expansion in recent years of the field of membrane raft-like domain formation [11, 132, 133] imposes the compelling need for understanding the effect of lipid bilayer composition on membrane properties. Cholesterol, a ubiquitous species in eukaryotic membranes, is an important component in raft-like domains in cells and in vesicles, which motivates studies aimed at understanding its influence on the mechanical properties and stability of membranes.

A widely accepted view in the past regarded cholesterol as a stiffening agent in membranes. The conventional belief was that cholesterol orders the acyl chains in fluid membranes and increases the bending stiffness. This concept was supported by observations of lipids such as stearoyloleoylphosphatidylcholine (SOPC) [134, 135], dimyristoylphosphatidylcholine [53, 136], and palmitoyloleoylphosphatidylcholine (not only in mixtures with cholesterol but also with other sterols) [137]. However, as demonstrated recently [55, 138–140], the bending rigidity of membranes made of dioleoylphosphatidylcholine (DOPC) and cholesterol does not show any significant correlation with the cholesterol content. This suggests that the effect of cholesterol is not universal, but rather specific to the lipid

architecture with respect to unsaturation and acyl chain length, and probably the lipid interfacial region.

The influence of cholesterol on other properties relevant for the stability and electroporation of membranes has not been studied extensively. The inverted-cone shape of this molecule should prevent it from locating at the rim of pores in membranes. Thus, the presence of cholesterol would require more energy to rearrange the lipids along the pore walls leading to an effective increase in the edge tension. Observations in this direction have been reported [141]. In [141] the pores were induced by strong illumination of giant vesicles inducing membrane stretching. Electroporation of giant vesicles and observation on the dynamics of pore closure also supported the notion of cholesterol increasing the edge tension [110]. The associated implication is that the lifetime of pores in such membranes is shorter (as defined above, the pore lifetime is inversely proportional to the edge tension; see Section 7.2). Note that both studies mentioned above on the effect of cholesterol on pore stability [110, 141] were performed using DOPC membranes. It remains to be clarified whether the tendency will be preserved when other lipids with different degrees of saturation are considered.

Another peculiarity of DOPC–cholesterol GUVs is that they are destabilized and collapse when exposed to DC pulses at which cholesterol-free vesicles (e.g., made of egg phosphatidylcholine (egg PC) or pure DOPC) preserve their stability and only porate and reseal. The cholesterol-doped GUVs burst and disintegrated in a fashion reminiscent of that of charged membranes [142] (see Figure 7.6 for an example of a collapsing charged vesicle). As a quantitative characteristic of mem-

Colour Figure

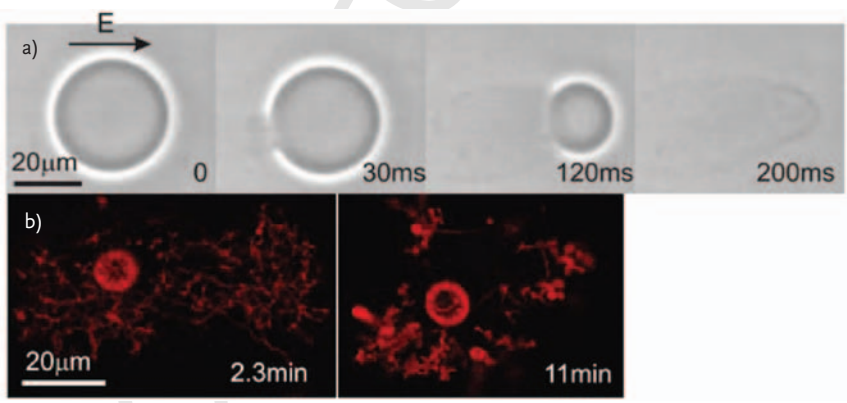

Figure 7.6 Bursting of charged vesicles subjected to electric pulses. The time after the beginning of the pulse is marked on each image. (a) Phase contrast microscopy snapshots from fast-camera observation of a vesicle in salt solution subjected to a pulse with field strength of 120 kV m^{-1} and duration of 200 μs. The field direction is indicated in the first snapshot. The vesicle bursts and disintegrates. (b) Confocal microscopy cross sections of a vesicle that has been subjected to an electric pulse and after bursting has rearranged into a network of tubes and smaller vesicles. Adapted from [42] by permission of the Royal Society of Chemistry.

brane stability in electric fields one can consider the critical transmembrane potential, Ψ_c, at which poration occurs. Following [80], at the moment of maximally expanded pore, one can define the critical transmembrane potential as $\Psi_c = 1.5RE\cos\theta_p$, where R is the initial vesicle radius before poration, E is the field magnitude, and θ_p is the inclination angle defining the location of the pore edge with respect to the vesicle center. This expression can be presented as $\Psi_c = 1.5E\left(R^2 - r_{pore}^2\right)^{1/2}$, where r_{pore} is the maximal pore size. Thus, measuring r_{pore} immediately after applying a pulse with a field strength E provides a *rough* estimate for the critical transmembrane poration Ψ_c. While cholesterol-free membranes made of different lipids porate at similar values of Ψ_c of around 0.9 V, the addition of 17 mol% cholesterol to DOPC bilayers decreases the critical transmembrane potential to around 0.7 V, that is, destabilizes these membranes when exposed to an electric pulse [110]. This finding implies that cholesterol lowers the lysis tension of DOPC membranes. This observation is interesting and unexpected having in mind the somewhat opposite effect of cholesterol observed on SOPC giant vesicles [59, 103], where it was found to increase the critical poration threshold Ψ_c. On the contrary, DPPC vesicles doped with cholesterol appear to porate at transmembrane potentials lower than those of pure DPPC membranes [143]. Finally, for egg PC planar membranes [144] and vesicles [143] no effect of cholesterol on the critical permeabilization potential was observed.

The origin of the cholesterol-induced changes to the critical poration potential could be sought in its effect on altering the membrane conductivity justified in detail in [143]. This behavior may be related to lipid ordering, which may occur to a different extent depending on the type of lipid. In summary, cholesterol, which alters the hydrophobic core of the bilayer, affects the membrane stability in a different fashion depending on the specific molecular architecture of the lipid building the membrane.

7.4.3
Membranes with Charged Lipids

As discussed in Section 7.2, strong electric pulses applied to single-component giant vesicles made of zwitterionic lipids like PCs induce the formation of pores, which reseal within tens of milliseconds. When negatively charged lipids, like phosphatidylglycerol (PG) or phosphatidylserine, are present in a membrane a very different response of the vesicles can be observed, partially influenced by the medium conditions [142].

In buffered solutions containing ethylenediaminetetraacetic acid, PC:PG vesicles with molar ratios 9 : 1, 4 : 1, and 1 : 1 behave in the same way as pure PC vesicles, that is, the pulses induce opening of macropores with a diameter up to about 10 μm, which reseal within tens of milliseconds. In nonbuffered solution, the membranes with low fractions of charged lipids (9 : 1 and 4 : 1) retain this behavior, but for membrane composition of 1 : 1 PC:PG, the vesicles collapse and disintegrate after electroporation [142] (see Figure 7.6). Typically, one macropore forms and expands in the first 50–100 ms at a very high speed of approximately 1 mm s^{-1}.

The entire vesicle content is released seen as darker fluid in Figure 7.6. The bursting is followed by restructuring of the membrane into what seem to be interconnected bilayer fragments in the first seconds, and a tether-like structure in the first minute. Then the membrane stabilizes into interconnected micrometer-sized tubules and small vesicles. Similar behavior is observed for vesicles prepared from lipid extracts from the plasma membrane of red blood cells which also contain a fraction of charged lipids [142]. These observations suggest that vesicle bursting and membrane instability are related to the amount of charged lipid in the bilayer as theoretically predicted in earlier studies [145–147].

As mentioned above, observations of GUVs prepared from lipid extracts from the plasma membrane of red blood cells show a response similar to that of vesicles prepared from synthetic charged lipids. Thus, one would intuitively expect that cells should exhibit similar bursting behavior. However, cell membranes are subjected to internal mechanical constraints imposed by the cytoskeleton, which prevents their disintegration even if their membranes are prone to disruption when exposed to strong DC pulses. Instead, the pores in the cell membrane are stable for a long time [148] and can either lead to cell death by lysis or reseal depending on the media [149, 150]. The latter is the key to efficient electroporation-based protocols for drug or gene transfer in cells. The results discussed in this section suggest that membrane charge might be an important, but not yet well understood, regulating agent in these protocols.

7.5
Application of Vesicle Electroporation

In this section some application aspects of giant vesicle electroporation are considered. In particular, it will be demonstrated that creating macropores in GUVs and observing their closing dynamics can be successfully applied to the evaluation of material properties of membranes. While in Section 7.4.2 we saw that such experiments can be used to characterize membrane stability in terms of the critical poration potential Ψ_c, here we will find out how one can also evaluate the edge tension of porated membranes. In addition, another application based on electroporation, namely vesicle electrofusion, is introduced whereby the use of GUVs as microreactors suitable for the synthesis of nanoparticles is demonstrated.

7.5.1
Measuring Membrane Edge Tension from Vesicle Electroporation

Upon poration, the lipid molecules in a bilayer reorient so that their polar heads can line the pore walls and form a hydrophilic pore [151]. The energetic penalty per unit length for this reorganization is described by the edge tension, which emerges from the physicochemical properties and the amphiphilic nature of lipids. It also gives rise to a force driving the closure of transient pores, playing a crucial role in membrane resealing mechanisms taking place after physical pro-

tocols for drug delivery, such as sonoporation [152] or electroporation [153]. Being able to experimentally measure the edge tension is thus of significant interest for understanding various biological events and physicochemical processes in membranes. However, only a few experimental methods have been developed to directly assess this physical quantity. Among them, an elegant approach was based on rapid freezing of cells with a controlled time delay after electroporation, and examining the pores with electron microscopy [154, 155]. This method, however, provides a static picture of the porated membrane and there is a danger of ice crystal damage.

Only a few previous studies have employed GUVs for estimating edge tension. Observations of open cylindrical giant vesicles exposed to AC fields [109] provided an estimate for the edge tension, but this technique did not allow for good control over the system. In another work, vesicles were porated with an electric pulse, and the pores were kept open by externally adjusting the membrane tension with a micropipette [103]. Even though solid, this approach requires the use of sophisticated equipment like a set-up for vesicle micropipette aspiration. GUVs were also used in [141, 156], where the pore closure dynamics was analyzed in light of a theory developed earlier [44]. However, for the direct visualization of pore closure, the use of viscous glycerol solutions and fluorescent dyes in the membrane was required, both of which potentially influence the edge tension. (The theoretical approach in [44] was also applied to experiments where the membrane was disrupted by laser ablation in [157], but the results of the latter study seem questionable since laser ablation is associated with local evaporation; indeed, the images provided in this work suggest the formation of bubbles in the sample rather than pores in the membrane.)

A much simpler approach introduced recently is based on the electroporation of giant vesicles and observation of the pore closure dynamics with fast digital imaging [110, 158]. The analysis of the pore dynamics was based on the theoretical work of Brochard-Wyart *et al.* [44]. The process of pore closure was observed under phase contrast microscopy with a high-speed digital camera (the acquisition speed was typically above 1000 fps). In this way, the need to use viscous solutions to slow down the system dynamics was avoided and the application of fluorescent dyes to visualize the vesicles as in [104, 141, 156] was not necessary. Note that both glycerol and fluorescent markers may influence the measured value for the edge tension. Vesicle electroporation was induced by applying electric pulses of 5 ms duration and field strength in the range 20–80 kV m^{-1}. The pore dynamics typically consisted of four stages: growing, stabilization at some maximal pore radius, slow decrease in pore size, and fast closure (e.g., data in Figure 7.7). The third stage of slow pore closure is the one that can be used to determine the membrane edge tension applying the dependence derived in [44]:

$$R^2 \ln(r) = -\frac{2\gamma}{3\pi\eta} t + C \tag{7.5}$$

where R and r are the vesicle and pore radii, respectively, γ is the edge tension, η is the viscosity of the aqueous medium, t is time, and C is a constant depending

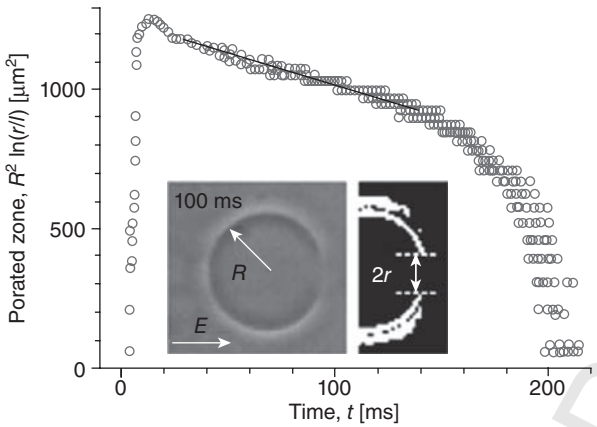

Figure 7.7 Evolution of the porated region in an egg PC vesicle as characterized by $R^2\ln(r/l)$ as a function of time t (see Eq. (7.5); note that to avoid plotting a dimensional value in the logarithmic term, we have introduced $l = 1\,\mu m$). The open circles are experimental data and the solid line is a linear fit, whose slope yields the edge tension γ. The inset shows a raw image (left) of a porated vesicle with a radius of 17 μm 100 ms after being exposed to an electric pulse with duration of 5 ms and amplitude of 50 kV m^{-1}. The field direction is indicated with an arrow. The right-hand side of the inset is an enhanced and processed image of the vesicle half facing the cathode. The inner white contour corresponds to the location of the membrane. The pore radius is schematically indicated.

on the maximal pore radius reached. Then, one only has to consider the linear part of $R^2\ln(r)$ as a function of time corresponding to the slow closure stage. Linear fit of this part is characterized by a slope a and the edge tension γ is estimated from the relation $\gamma = -(3/2)\pi\eta a$. Figure 7.7 illustrates the analysis performed on one egg PC vesicle. Measurements on many vesicles yielded an average value of $\gamma = 14.3$ pN for the edge tension of such membranes.

Using this approach, one can measure the edge tension in membranes of various compositions, thus characterizing the stability of pores in these membranes, and evaluate the effect of various inclusions. For example, it was found that the addition of cholesterol to DOPC membranes increases the edge tension confirming previously reported results [141]. The inverted-cone shape of cholesterol prevents it from locating at the rim of pores. Thus, the presence of cholesterol requires more energy to rearrange the lipids along the pore walls increasing the edge tension. Surprisingly, doping DOPC membranes with another cone-shaped type of lipid like dioleoylphosphatidylethanolamine (DOPE) was found to decrease the edge tension, that is, DOPE has a pore-stabilizing effect [110]. Presumably, the molecular architecture of phosphatidylethanolamine (PE)–lipids leading to their tendency to form an inverted hexagonal phase, which facilitates fusion and vesicle leakage (e.g., [159]), is also responsible for stabilizing pores. A plausible explanation for this behavior is also provided by the propensity of PE to form interlipid hydrogen bonds [160, 161], that is, inter-PE hydrogen bonding in the pore region can effectively stabilize pores.

As demonstrated above, the edge tension is a sensitive parameter, which effectively characterizes the stability of pores in membranes. Compiling a database for the effect of various types of membrane inclusions will be useful for understanding the lifetime of pores in membranes with more complex compositions, which is important for achieving control over medical applications for drug and gene delivery in cells.

7.5.2 Vesicle Electrofusion

The phenomenon of membrane electrofusion is of particular interest, because of its widespread use in cell biology and biotechnology (e.g., [162–164] and the references cited therein). The application of electrofusion to cells can lead to the creation of multinucleated viable cells with new properties (this phenomenon is also known as hybridization) (e.g., [164]). In addition, electroporation and electrofusion are often used to introduce molecules like proteins, foreign genes (plasmids), antibodies, and drugs into cells.

When a DC pulse is applied to a couple of fluid-phase vesicles, which are in contact and oriented in the direction of the field, electrofusion can be observed. Vesicle orientation (and even alignment into pearl chains) can be achieved by application of an AC field to a vesicle suspension. This phenomenon is also observed with cells [164, 165] and is due to dielectric screening of the field. When the suspension is dilute, two vesicles can be brought together via the AC field and aligned. A subsequent application of a DC pulse to such a vesicle couple can lead to fusion. The necessary condition is that poration is induced in the contact area between the two vesicles. The possible steps of the electrofusion of two membranes are schematically illustrated in Figure 7.8a. In Sections 7.5.2.1 and 7.5.2.2, consideration will be given to the fusion of vesicles with different membrane composition or different composition of the enclosed solutions.

7.5.2.1 Fusing Vesicles with Identical or Different Membrane Composition

Membrane fusion is a fast process. The time needed for the formation of a fusion neck can be rather short as demonstrated by electrophysiological methods applied to the fusion of small vesicles with cell membranes [166–169]. The time evolution of the observed membrane capacitance indicates that the formation of the fusion neck is presumably faster than 100 µs. Direct observation of the fusion of giant vesicles recently confirmed this finding and suggesting that this time is even shorter [36, 37]. An example of a few snapshots taken from the electrofusion of two GUVs with identical membrane compositions and in the presence of salt is given in Figure 7.8b. The overall deformation of each vesicle as seen in the second snapshot corresponds to the spherocylindrical shapes as observed with individual vesicles in the presence of salt (see Section 7.4.1). From such micrographs, one can measure the fusion neck diameter, denoted by L in Figures 7.8a and 7.8b, and follow the dynamics of its expansion as shown in Figure 7.8c. From the data, two stages of the fusion process can be distinguished (note that the data are displayed in a semi-logarithmic plot): an early stage, which is very fast and with average

Colour Figure

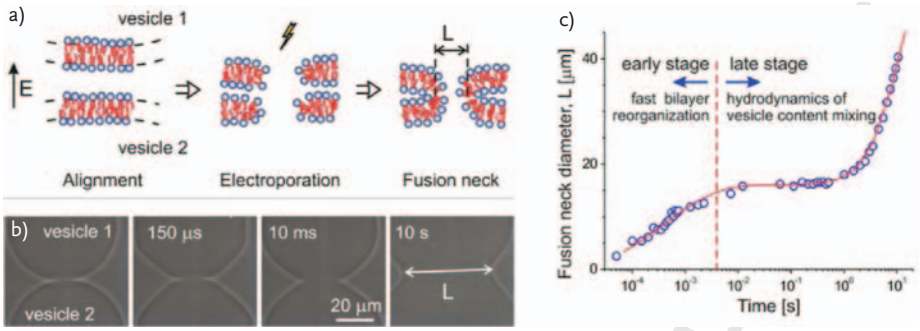

Figure 7.8 Membrane electrofusion. (a) Schematic of the possible steps of the electrofusion process: two lipid vesicles are brought into contact (only the membranes in the contact zone of the vesicles are sketched), followed by electroporation and formation of a fusion neck of diameter *L*. The pore sizes are not to scale but almost an order of magnitude larger than the bilayer thickness. (b) Micrographs from the electrofusion of a vesicle couple. Only segments of the vesicles are visible. The external solution contains 1 mM NaCl, which causes flattening of the vesicle walls in the second snapshot (see Section 7.4.1). The amplitude of the DC pulse was 240 kV m^{-1}, and its duration was 120 µs. The time after the beginning of the pulse is indicated on the snapshots. (c) Time evolution of the fusion neck diameter, *L*, formed between two vesicles with radii of about 15 µm. The solid curve is a guide to the eye. The vertical dashed line indicates the border between the two stages in the fusion dynamics. Adapted from [41] by permission of the Royal Society of Chemistry.

expansion velocity of about 2×10^4 µm s^{-1}, followed by a later slower stage with an expansion rate that is orders of magnitude smaller (about 2 µm s^{-1}). The early stage is governed by fast relaxation of the membrane tension built during the pulse, whereby the dissipation occurs in the bilayer. Essentially, the driving forces here are the same as those responsible for the relaxation dynamics of nonporated vesicles (as characterized by τ_1 in Section 7.2). Thus, the characteristic time for this early stage of fusion, τ_{early}, can be expressed as $\tau_{early} \sim \eta_D/\sigma$, where the membrane tension σ should be close to the tension of rupture σ_{lys}. Thus for τ_{early} one obtains a value of 100 µs, which is in agreement with the experimental observations for the time needed to complete the early stage of fusion. Linear extrapolation of the data in the early stage predicts that the formation of a fusion neck with a diameter of about 10 nm should occur within a time period of about 250 ns [37]. It is quite remarkable that this time scale of the order of 200 ns was also obtained from computer simulations of a vesicle fusing with a tense membrane segment [169].

In the later stage of fusion, the neck expansion velocity slows down by more than two orders of magnitude. Here the dynamics is mainly governed by the displacement of the volume of fluid around the fusion neck between the fused vesicles. The restoring force is related to the bending elasticity of the lipid bilayer [36, 37].

Fusing two vesicles with membranes of different composition can provide a promising tool for studying raft-like domains in membranes [11, 12, 133, 170, 171].

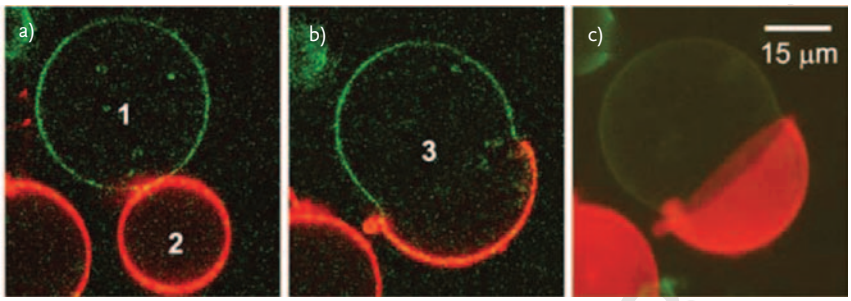

Colour Figure

Figure 7.9 Creating a multidomain vesicle by electrofusion of two vesicles with different membrane composition as observed with fluorescence microscopy. (a, b) Images acquired with confocal microscopy scans nearly at the equatorial plane of the fusing vesicles. (a) Vesicle 1 is made of sphingomyelin and cholesterol (7:3) and labeled with one fluorescent dye (green). Vesicle 2 is composed of dioleoylphosphatidylcholine and cholesterol (8:2) and labeled with another fluorescent dye (red). (b) The two vesicles were subjected to an electric pulse (220 kV m^{-1}, duration 300 µs) and fused to form vesicle 3. Because the lipids with this final membrane composition form immiscible fluid phases, the resulting vesicle has two domains. (c) A three-dimensional image projection of vesicle 3 with the two domains formed from vesicles 1 and 2. Adapted from [41] by permission of the Royal Society of Chemistry.

In particular, vesicle electrofusion is a very attractive experimental approach for producing multicomponent vesicles of well-defined composition [36]. One example for the fusion of two vesicles with different membrane composition is shown in Figure 7.9. To distinguish the vesicles according to their composition, two fluorescent markers have been used. In this particular example, one of the vesicles (vesicle 1) is composed of sphingomyelin and cholesterol in 7:3 molar ratio and labeled in green. The other vesicle (vesicle 2) is composed of DOPC and cholesterol in 8:2 molar ratio and labeled in red (with fluorescence microscopy, the two vesicle can be distinguished by their color). Thus, the membrane of the fused vesicle is a three-component one. At room temperature, this lipid mixture separates into two phases, liquid ordered (rich in sphingomyelin and cholesterol) and liquid disordered (rich in DOPC), which is why the final vesicle exhibits immiscible fluid domains. The exact composition of each of these domains is not well known because lipids may redistribute among the domains. However, from the domain area and the area of the initial vesicles before fusion, one can judge whether there is redistribution of cholesterol, and eventually calculate the actual domain composition.

7.5.2.2 Vesicle Electrofusion: Employing Vesicles as Microreactors

Vesicle fusion can be employed to scale down the interaction volume of a chemical reaction and reduce it to a few picoliters or less. In other words, fusion of two vesicles of different content can be used for the realization of a tiny microreactor [172–176]. The principle of fusion-mediated synthesis is simple: the starting reagents are separately loaded into different vesicles, and then the reaction is

triggered by the fusion of these vesicles, which allows the mixing of their contents. The success of this approach is guaranteed by two important factors. First, the lipid membrane is impermeable to the reactants such as ions or macromolecules. Second, fusion can be initiated by a variety of fusogens such as membrane stress [169, 177, 178], ions or synthetic fusogenic molecules [37, 179–181], fusion proteins [182], or electric fields [36, 176]. Among these approaches, electrofusion becomes increasingly important because of its reliable, fast, and easy handling. An immediate benefit of this strategy is that precise temporal control of the synthesis process can be easily achieved.

Synthesis of nanoparticles in such microreactors is of particular interest. Indeed, cells and microorganisms themselves have been reported to have the unique ability to synthesize inorganic nanoparticles such as CdS, ZnS, gold, and silver [183–185]. The tentative interpretation of this observation is related to the mediation ability of specific molecules such as inorganic-binding peptides [186]. Nevertheless, the underlying processes are still not well understood at the molecular scale. Therefore, attempts to perform similar reactions in simplified artificial systems become very important towards detailed exploration of biological synthesis mechanisms and biomimetic fabrication [185].

Although nanoparticle synthesis in vesicle nanoreactors has been well documented [187–190], much effort is still needed to perform such synthesis in GUVs so as to elucidate the biological mechanism of nanoparticle synthesis in cells and construct novel functional "artificial cells" for advanced technological applications. Other processes in giant vesicles occurring in their enclosed compartments or at the membrane surface have also been studied [172, 174, 175, 191–194]. Furthermore, one great and exclusive advantage of GUVs is that giant vesicles and the corresponding products of their interaction can be visualized in real time under a light microscope, providing the potential possibility for on-line monitoring of material growth at micrometer and submicrometer scales.

Success in this direction was recently reported for the synthesis of CdS quantum-like nanoparticles [176]. The protocol applied is schematically illustrated in Figure 7.10a. Two vesicle populations loaded with reactant A ($CdCl_2$) or B (Na_2S) are mixed in A-, B-free isotonic solution. To be able to distinguish the two vesicle types from each other, the membranes of A-loaded and B-loaded vesicles are labeled by small fractions of red and green fluorescent dyes, respectively, added to the main lipid building the membrane. Similar to pearl-chain formation in cell suspensions, the two types of vesicles self-align along the direction of an exogenous AC field. This field-induced self-arrangement makes reactive vesicles match well for the CdS synthesis reaction: half of the aligned vesicle couples are A–B couples. After that, a strong DC pulse is applied (typically pulses of 50–200 $kV\,m^{-1}$ field strength and 150–300 μs duration suffice) to initiate vesicle fusion and the reaction between A and B. The product, in this case quantum-dot-like CdS nanoparticles (with sizes between 4 and 8 nm as determined from transmission electron microscopy [176]), is visualized under laser excitation as a fluorescent bright spot in the fusion zone (see the second snapshot in Figure 7.10b). The intensity from this spot increases gradually from 0 s (the starting time point of electrofusion), and reaches maximum

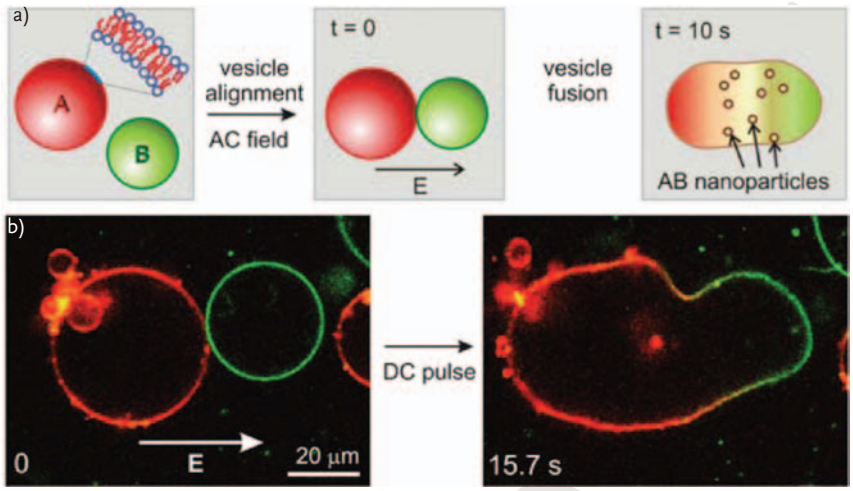

Colour Figure

Figure 7.10 Electrofusion of giant vesicles as a method for nanoparticle synthesis. (a) Schematic of the electrofusion protocol. Two populations of vesicles containing reactant A or B are mixed (in A- and B-free environment) and subjected to an AC field to align them in the direction of the field and bring them close together. A DC pulse initiates the electrofusion of the two vesicles and the reaction between A and B proceeds to the formation of nanoparticles encapsulated in the fused vesicle. (b) Confocal scans of vesicles loaded with 0.3 mM Na_2S (red) and 0.3 mM $CdCl_2$ (green) undergoing fusion. The direction of the field is indicated in the first snapshot. After fusion (second snapshot), fluorescence from the product is detected in the interior of the fused vesicle. The time after applying the pulse is indicated on the micrographs. Adapted from [176] by permission of Wiley-VCH Verlag.

around 10 s. One can therefore infer that the reaction begins at the electrofusion point and quickly reaches a balance around 10 s. Obviously, this protocol provides us with a visualizing analytical tool to follow the reaction kinetics with high temporal sensitivity. This novel and facile method is especially suitable for the on-line monitoring of ultrafast physicochemical processes such as photosynthesis, enzyme catalysis, and photopolymerization, which usually require complex and abstracted spectroscopy techniques at present. These results show that even without the mediation of biomacromolecules, nanoparticles can still be synthesized in biological compartments. This outcome provides a new insight in the developing research on biomineralization mechanisms.

7.6 Conclusions and Outlook

The issues addressed in this chapter demonstrate that cell-sized giant vesicles provide a very useful model for resolving various effects of electric fields on lipid membranes because vesicle dynamics can be directly observed with optical

microscopy. It has been shown that the vesicle response to electric fields can be interpreted and understood considering the basic mechanical properties of membranes.

Until recently, the dynamics of vesicle relaxation and poration, which occur on microsecond time scales, has eluded direct observation because the temporal resolution of optical microscopy observations with analog video technology is in the range of milliseconds. The recent use of fast digital imaging has helped us to characterize membrane deformation and poration and also to discover new features of the membrane response arising from the presence of charged lipids or cholesterol in the membrane and nanoparticles in the surrounding media, and to compare the response of gel-phase membranes to fluid-phase ones. Due to this high temporal resolution, new shape deformations, such as spherocylindrical ones, have been detected. The observations of vesicle fusion revealed the presence of two stages of the fusion process. Finally, a novel application of membrane electrofusion was introduced, which allows the construction of vesicles with fluid domains.

In conclusion, the reported observations demonstrate that giant vesicles as biomimetic membrane compartments can be of significant help to advance fundamental knowledge about the complex behavior of cells and membranes in electric fields and can inspire novel practical applications.

Acknowledgments

In preparing this chapter, I have profited from numerous experimental contributions and insightful discussions with skillful members of my group, and current and former collaborators. The work in the laboratory on vesicles in electric fields was initiated together with Karin A. Riske. I would also like to thank Roland L. Knorr, Natalya Bezlyepkina, Thomas Portet, Margarita Staykova, Peng Yang, Said Aranda, Marie Domange Jordö, Benjamin Klasczyk, and D. Duda. I also wish to acknowledge the valuable insight I got from the enlightening discussions with theoreticians like Reinhard Lipowsky, Petia M. Vlahovska, Tetsuya Yamamoto, and Rubèn S. Gracià.

References

1 Lasic, D.D. (ed.) (1993) *Liposomes: From Physics to Applications*, Elsevier, Amsterdam.
2 Luisi, P.L. and Walde, P. (eds) (2000) *Giant Vesicles*, John Wiley & Sons, Ltd, Chichester.
3 Dimova, R., Aranda, S., Bezlyepkina, N., Nikolov, V., Riske, K.A., and Lipowsky, R. (2006) A practical guide to giant vesicles. Probing the membrane nanoregime via optical microscopy. *Journal of Physics: Condensed Matter*, **18** (28), S1151–S1176.
4 Walde, P., Cosentino, K., Engel, H., and Stano, P. (2010) Giant vesicles: preparations and applications. *ChemBioChem*, **11** (7), 848–865.

5 Reeves, J.P. and Dowben, R.M. (1969) Formation and properties of thin-walled phospholipid vesicles. *Journal of Cellular Physiology*, **73** (1), 49–60.

6 Angelova, M.I. and Dimitrov, D.S. (1986) Liposome electroformation. *Faraday Discussions*, **81**, 303–311.

7 Akashi, K., Miyata, H., Itoh, H., and Kinosita, K. (1996) Preparation of giant liposomes in physiological conditions and their characterization under an optical microscope. *Biophysical Journal*, **71** (6), 3242–3250.

8 Akashi, K., Miyata, H., Itoh, H., and Kinosita, K. (1998) Formation of giant liposomes promoted by divalent cations: critical role of electrostatic repulsion. *Biophysical Journal*, **74** (6), 2973–2982.

9 Montes, L.R., Alonso, A., Goni, F.M., and Bagatolli, L.A. (2007) Giant unilamellar vesicles electroformed from native membranes and organic lipid mixtures under physiological conditions. *Biophysical Journal*, **93**, 3548–3554.

10 Pott, T., Bouvrais, H., and Meleard, P. (2008) Giant unilamellar vesicle formation under physiologically relevant conditions. *Chemistry and Physics of Lipids*, **154** (2), 115–119.

11 Lipowsky, R., and Dimova, R. (2003) Domains in membranes and vesicles. *Journal of Physics: Condensed Matter*, **15** (1), S31–S45.

12 Baumgart, T., Hess, S.T., and Webb, W.W. (2003) Imaging coexisting fluid domains in biomembrane models coupling curvature and line tension. *Nature*, **425** (6960), 821–824.

13 Veatch, S.L. and Keller, S.L. (2002) Organization in lipid membranes containing cholesterol. *Physical Review Letters*, **89** (26), 4.

14 Vitkova, V., Mader, M., and Podgorski, T. (2004) Deformation of vesicles flowing through capillaries. *Europhysics Letters*, **68** (3), 398–404.

15 Meleard, P., Gerbeaud, C., Pott, T., and Mitov, M.D. (2000) Electromechanical properties of model membranes and giant vesicle deformation, in *Giant Vesicles* (eds P.L. Luisi and P. Walde), John Wiley & Sons, Ltd, Chichester, pp. 185–205.

16 Dimova, R., Dietrich, C., Hadjiisky, A., Danov, K., and Pouligny, B. (1999) Falling ball viscosimetry of giant vesicle membranes: finite-size effects. *European Physical Journal B*, **12**, 589.

17 Wick, R., Walde, P., and Luisi, P.L. (1995) Light-microscopic investigations of the autocatalytic self-reproduction of giant vesicles. *Journal of the American Chemical Society*, **117** (4), 1435–1436.

18 Menger, F.M. and Gabrielson, K. (1994) Chemically-induced birthing and foraging in vesicle systems. *Journal of the American Chemical Society*, **116** (4), 1567–1568.

19 Takakura, K., Toyota, T., and Sugawara, T. (2003) A novel system of self-reproducing giant vesicles. *Journal of the American Chemical Society*, **125** (27), 8134–8140.

20 Zhu, T.F. and Szostak, J.W. (2009) Coupled growth and division of model protocell membranes. *Journal of the American Chemical Society*, **131** (15), 5705–5713.

21 Evans, E. and Metcalfe, M. (1984) Free-energy potential for aggregation of giant, neutral lipid bilayer vesicles by van der waals attraction. *Biophysical Journal*, **46** (3), 423–426.

22 Evans, E. (1991) Entropy-driven tension in vesicle membranes and unbinding of adherent vesicles. *Langmuir*, **7** (9), 1900–1908.

23 Dietrich, C., Angelova, M.I., and Pouligny, B. (1997) Adhesion of latex spheres to giant phospholipid vesicles: statics and dynamics. *Journal de Physique II France*, **7**, 1651–1682.

24 Gruhn, T., Franke, T., Dimova, R., and Lipowsky, R. (2007) Novel method for measuring the adhesion energy of vesicles. *Langmuir*, **23** (10), 5423–5429.

25 Fang, N., Chan, V., and Wan, K.T. (2003) The effect of electrostatics on the contact mechanics of adherent phospholipid vesicles. *Colloids and Surfaces B*, **27** (1), 83–94.

26 Li, Y., Lipowsky, R., and Dimova, R. (2008) Transition from complete to partial wetting within membrane compartments. *Journal of the American Chemical Society*, **130** (37), 12252–12253.

27 Kusumaatmaja, H., Li, Y., Dimova, R., and Lipowsky, R. (2009) Intrinsic contact angle of aqueous phases at membranes and vesicles. *Physical Review Letters*, **103** (23), 238103–238104.

28 Kas, J. and Sackmann, E. (1991) Shape transitions and shape stability of giant phospholipid-vesicles in pure water induced by area-to-volume changes. *Biophysical Journal*, **60** (4), 825–844.

29 Dobereiner, H.G., Kas, J., Noppl, D., Sprenger, I., and Sackmann, E. (1993) Budding and fission of vesicles. *Biophysical Journal*, **65** (4), 1396–1403.

30 Peterlin, P., Arrigler, V., Kogej, K., Svetina, S., and Walde, P. (2009) Growth and shape transformations of giant phospholipid vesicles upon interaction with an aqueous oleic acid suspension. *Chemistry and Physics of Lipids*, **159** (2), 67–76.

31 Staneva, G., Seigneuret, M., Koumanov, K., Trugnan, G., and Angelova, M.I. (2005) Detergents induce raft-like domains budding and fission from giant unilamellar heterogeneous vesicles – a direct microscopy observation. *Chemistry and Physics of Lipids*, **136** (1), 55–66.

32 Inaoka, Y. and Yamazaki, M. (2007) Vesicle fission of giant unilamellar vesicles of liquid-ordered-phase membranes induced by amphiphiles with a single long hydrocarbon chain. *Langmuir*, **23** (2), 720–728.

33 Pantazatos, D.P. and MacDonald, R.C. (1999) Directly observed membrane fusion between oppositely charged phospholipid bilayers. *Journal of Membrane Biology*, **170** (1), 27–38.

34 Lei, G.H. and MacDonald, R.C. (2003) Lipid bilayer vesicle fusion: intermediates captured by high-speed microfluorescence spectroscopy. *Biophysical Journal*, **85** (3), 1585–1599.

35 Zhou, Y.F. and Yan, D.Y. (2005) Real-time membrane fusion of giant polymer vesicles. *Journal of the American Chemical Society*, **127** (30), 10468–10469.

36 Riske, K.A., Bezlyepkina, N., Lipowsky, R., and Dimova, R. (2006) Electrofusion of model lipid membranes viewed with high temporal resolution. *Biophysical Review Letters*, **1** (4), 387–400.

37 Haluska, C.K., Riske, K.A., Marchi-Artzner, V., Lehn, J.M., Lipowsky, R., and Dimova, R. (2006) Time scales of membrane fusion revealed by direct imaging of vesicle fusion with high temporal resolution. *Proceedings of the National Academy of Sciences of the USA*, **103** (43), 15841–15846.

38 Abkarian, M. and Viallat, A. (2008) Vesicles and red blood cells in shear flow. *Soft Matter*, **4** (4), 653–657.

39 Raphael, R. and Waugh, R. (1996) Accelerated interleaflet transport of phosphatidylcholine molecules in membranes under deformation. *Biophysical Journal*, **71**, 1374–1388.

40 Evans, E. and Rawicz, W. (1997) Elasticity of "fuzzy" biomembranes. *Physical Review Letters*, **79** (12), 2379–2382.

41 Dimova, R., Riske, K.A., Aranda, S., Bezlyepkina, N., Knorr, R.L., and Lipowsky, R. (2007) Giant vesicles in electric fields. *Soft Matter*, **3** (7), 817–827.

42 Dimova, R., Bezlyepkina, N., Jordo, M.D., Knorr, R.L., Riske, K.A., Staykova, M., Vlahovska, P.M., Yamamoto, T., Yang, P., and Lipowsky, R. (2009) Vesicles in electric fields: some novel aspects of membrane behavior. *Soft Matter*, **5** (17), 3201–3212.

43 Dimova, R., Pouligny, B., and Dietrich, C. (2000) Pretransitional effects in dimyristoylphosphatidylcholine vesicle membranes: optical dynamometry study. *Biophysical Journal*, **79** (1), 340–356.

44 Brochard-Wyart, F., de Gennes, P.G., and Sandre, O. (2000) Transient pores in stretched vesicles: role of leak-out. *Physica A*, **278** (1–2), 32–51.

45 Marsh, D. (2006) Elastic curvature constants of lipid monolayers and bilayers. *Chemistry and Physics of Lipids*, **144** (2), 146–159.

46 Seifert, U. and Lipowsky, R. (1995) Morphology of vesicles, in *Structure and Dynamics of Membranes (Handbook of Biological Physics)* (eds R. Lipowsky and E. Sackmann), Elsevier, Amsterdam, pp. 403–463.

47 Rawicz, W., Olbrich, K.C., McIntosh, T., Needham, D., and Evans, E. (2000) Effect of chain length and unsaturation

on elasticity of lipid bilayers. *Biophysical Journal*, **79** (1), 328–339.
48 Brochard, F. and Lennon, J.F. (1975) Frequency spectrum of flicker phenomenon in erythrocytes. *Journal of Physics*, **36** (11), 1035–1047.
49 Schneider, M.B., Jenkins, J.T., and Webb, W.W. (1984) Thermal fluctuations of large quasi-spherical bimolecular phospholipid-vesicles. *Journal of Physics*, **45** (9), 1457–1472.
50 Engelhardt, H., Duwe, H.P., and Sackmann, E. (1985) Bilayer bending elasticity measured by Fourier analysis of thermally excited surface undulations of flaccid vesicles. *Journal of Physics Letters*, **46** (8), L395–L400.
51 Bivas, I., Hanusse, P., Bothorel, P., Lalanne, J., and Aguerrechariol, O. (1987) An application of the optical microscopy to the determination of the curvature elastic-modulus of biological and model membranes. *Journal of Physics*, **48** (5), 855–867.
52 Faucon, J.F., Mitov, M.D., Meleard, P., Bivas, I., and Bothorel, P. (1989) Bending elasticity and thermal fluctuations of lipid membranes – theoretical and experimental requirements. *Journal of Physics*, **50** (17), 2389–2414.
53 Duwe, H.P., Kaes, J., and Sackmann, E. (1990) Bending elastic moduli of lipid bilayers – modulation by solutes. *Journal of Physics*, **51** (10), 945–962.
54 Henriksen, J.R., and Ipsen, J.H. (2002) Thermal undulations of quasi-spherical vesicles stabilized by gravity. *European Physical Journal E*, **9** (4), 365–374.
55 Gracia, R.S., Bezlyepkina, N., Knorr, R.L., Lipowsky, R., and Dimova, R. (2010) Effect of cholesterol on the rigidity of saturated and unsaturated membranes: fluctuation and electrodeformation analysis of giant vesicles. *Soft Matter*, **6** (7), 1472–1482.
56 Mecke, K.R., Charitat, T., and Graner, F. (2003) Fluctuating lipid bilayer in an arbitrary potential: theory and experimental determination of bending rigidity. *Langmuir*, **19** (6), 2080–2087.
57 Lee, C.H., Lin, W.C., and Wang, J.P. (2001) All-optical measurements of the bending rigidity of lipid-vesicle membranes across structural phase transitions. *Physical Review E*, **64** (2), 020901.
58 Needham, D. and Evans, E. (1988) Structure and mechanical properties of giant lipid (DMPC) vesicle bilayers from 20-degrees-C below to 10-degrees-C above the liquid-crystal crystalline phase transition at 24-degrees-C. *Biochemistry*, **27** (21), 8261–8269.
59 Needham, D. and Hochmuth, R.M. (1989) Electro-mechanical permeabilization of lipid vesicles – role of membrane tension and compressibility. *Biophysical Journal*, **55** (5), 1001–1009.
60 Olbrich, K., Rawicz, W., Needham, D., and Evans, E. (2000) Water permeability and mechanical strength of polyunsaturated lipid bilayers. *Biophysical Journal*, **79** (1), 321–327.
61 Evans, E., Heinrich, V., Ludwig, F., and Rawicz, W. (2003) Dynamic tension spectroscopy and strength of biomembranes. *Biophysical Journal*, **85** (4), 2342–2350.
62 Evans, E. and Needham, D. (1987) Physical properties of surfactant bilayer membranes – thermal transitions, elasticity, rigidity, cohesion, and colloidal interactions. *Journal of Physical Chemstry*, **91** (16), 4219–4228.
63 Boal, D. (ed.) (2002) *Mechanics of the Cell*, Cambridge University Press, Cambridge.
64 Aranda, S., Riske, K.A., Lipowsky, R., and Dimova, R. (2008) Morphological transitions of vesicles induced by alternating electric fields. *Biophysical Journal*, **95** (2), L19–L21.
65 Winterhalter, M. and Helfrich, W. (1988) Deformation of spherical vesicles by electric fields. *Journal of Colloid and Interface Science*, **122** (2), 583–586.
66 Hyuga, H., Kinosita, K., and Wakabayashi, N. (1991) Transient and steady-state deformations of a vesicle with an insulating membrane in response to step-function or alternating electric fields. *Japanese Journal of Applied Physics Part 1*, **30** (10), 2649–2656.
67 Mitov, M.D., Meleard, P., Winterhalter, M., Angelova, M.I., and Bothorel, P. (1993) Electric-field-dependent thermal

fluctuations of giant vesicles. *Physical Review E*, **48** (1), 628–631.
68 Hyuga, H., Kinosita, K., and Wakabayashi, N. (1993) Steady-state deformation of a vesicle in alternating electric fields. *Bioelectrochemistry and Bioenergetics*, **32** (1), 15–25.
69 Peterlin, P., Svetina, S., and Zeks, B. (2007) The prolate-to-oblate shape transition of phospholipid vesicles in response to frequency variation of an AC electric field can be explained by the dielectric anisotropy of a phospholipid bilayer. *Journal of Physics: Condensed Matter*, **19** (13), 136220.
70 Peterlin, P. (2010) Frequency-dependent electrodeformation of giant phospholipid vesicles in AC electric field. *Journal of Biological Physics*, **36**, 339–354.
71 Vlahovska, P.M., Gracia, R.S., Aranda-Espinoza, S., and Dimova, R. (2009) Electrohydrodynamic model of vesicle deformation in alternating electric fields. *Biophysical Journal*, **96** (12), 4789–4803.
72 Yamamoto, T., Aranda-Espinoza, S., Dimova, R., and Lipowsky, R. (2010) Stability of spherical vesicles in electric fields. *Langmuir*, **26**, 12390–12407.
73 Gao, L.T., Feng, X.Q., and Gao, H.J. (2009) A phase field method for simulating morphological evolution of vesicles in electric fields. *Journal of Computational Physics*, **228** (11), 4162–4181.
74 Gao, L.T., Liu, Y., Qin, Q.H., and Feng, X.Q. (2010) Morphological stability analysis of vesicles with mechanical-electrical coupling effects. *Acta Mechanica Sinica*, **26** (1), 5–11.
75 Niggemann, G., Kummrow, M., and Helfrich, W. (1995) The bending rigidity of phosphatidylcholine bilayers–dependences on experimental method, sample cell sealing and temperature. *Journal of Physics II*, **5** (3), 413–425.
76 Peterlin, P., Svetina, S., and Zeks, B. (2000) The frequency dependence of phospholipid vesicle shapes in an external electric field. *Pfluegers Archiv/European Journal of Physiology*, **439**, R139–R140.
77 Antonova, K., Vitkova, V., and Mitov, M.D. (2010) Deformation of giant vesicles in AC electric fields-Dependence of the prolate-to-oblate transition frequency on vesicle radius. *Europhysics Letters*, **89** (3), 38004.
78 Staykova, M., Lipowsky, R., and Dimova, R. (2008) Membrane flow patterns in multicomponent giant vesicles induced by alternating electric fields. *Soft Matter*, **4** (11), 2168–2171.
79 Lecuyer, S., Ristenpart, W.D., Vincent, O., and Stone, H.A. (2008) Electrohydrodynamic size stratification and flow separation of giant vesicles. *Applied Physics Letters*, **92** (10), 104105.
80 Neumann, E., Sowers, A.E., and Jordan, C. (eds) (1989) *Electroporation and Electrofusion in Cell Biology*, Plenum, New York.
81 Kotnik, T., Pucihar, G., Rebersek, M., Miklavcic, D., and Mir, L.M. (2003) Role of pulse shape in cell membrane electropermeabilization. *Biochimica et Biophysica Acta*, **1614** (2), 193–200.
82 Tekle, E., Astumian, R.D., and Chock, P.B. (1991) Electroporation by using bipolar oscillating electric-field–an improved method for DNA transfection of Nih 3t3 cells. *Proceedings of the National Academy of Sciences of the USA*, **88** (10), 4230–4234.
83 Hyuga, H., Kinosita, K., and Wakabayashi, N. (1991) Deformation of vesicles under the influence of strong electric-fields. *Japanese Journal of Applied Physics Part 1*, **30** (5), 1141–1148.
84 Hyuga, H., Kinosita, K., and Wakabayashi, N. (1991) Deformation of vesicles under the influence of strong electric fields. 2. *Japanese Journal of Applied Physics Part 1*, **30** (6), 1333–1335.
85 Sokirko, A., Pastushenko, V., Svetina, S., and Zeks, B. (1994) Deformation of a lipid vesicle in an electric-field–a theoretical study. *Bioelectrochemistry and Bioenergetics*, **34** (2), 101–107.
86 Neumann, E., Kakorin, S., and Toensing, K. (1998) Membrane electroporation and electromechanical deformation of vesicles and cells. *Faraday Discussions*, **111** (111), 111–125.
87 Griese, T., Kakorin, S., and Neumann, E. (2002) Conductometric and electrooptic relaxation spectrometry of lipid vesicle electroporation at high

fields. *Physical Chemistry Chemical Physics*, **4** (7), 1217–1227.
88 Kakorin, S. and Neumann, E. (2002) Electrooptical relaxation spectrometry of membrane electroporation in lipid vesicles. *Colloids and Surfaces A*, **209** (2–3), 147–165.
89 Riske, K.A. and Dimova, R. (2005) Electro-deformation and poration of giant vesicles viewed with high temporal resolution. *Biophysical Journal*, **88** (2), 1143–1155.
90 Riske, K.A. and Dimova, R. (2005) Timescales involved in electro-deformation, poration and fusion of giant vesicles resolved with fast digital imaging. *Biophysical Journal*, **88** (1), 241A–241A.
91 Kinosita, K., Ashikawa, I., Saita, N., Yoshimura, H., Itoh, H., Nagayama, K., and Ikegami, A. (1988) Electroporation of cell-membrane visualized under a pulsed-laser fluorescence microscope. *Biophysical Journal*, **53** (6), 1015–1019.
92 Abidor, I.G., Arakelyan, V.B., Chernomordik, L.V., Chizmadzhev, Y.A., Pastushenko, V.F., and Tarasevich, M.R. (1979) Electrical breakdown of bilayer lipid-membranes. 1. Main experimental facts and their qualitative discussion. *Bioelectrochemistry and Bioenergetics*, **6** (1), 37–52.
93 Simon, S.A. and McIntosh, T.J. (1986) Depth of water penetration into lipid bilayers. *Methods in Enzymology*, **127**, 511–521.
94 Nagle, J.F. and Tristram-Nagle, S. (2000) Structure of lipid bilayers. *Biochimica et Biophysica Acta*, **1469** (3), 159–195.
95 Hibino, M., Shigemori, M., Itoh, H., Nagayama, K., and Kinosita, K. (1991) Membrane conductance of an electroporated cell analyzed by submicrosecond imaging of transmembrane potential. *Biophysical Journal*, **59** (1), 209–220.
96 Akinlaja, J. and Sachs, F. (1998) The breakdown of cell membranes by electrical and mechanical stress. *Biophysical Journal*, **75** (1), 247–254.
97 Portet, T., Febrer, F.C.I., Escoffre, J.M., Favard, C., Rols, M.P., and Dean, D.S. (2009) Visualization of membrane loss during the shrinkage of giant vesicles under electropulsation. *Biophysical Journal*, **96** (10), 4109–4121.
98 Tsong, T.Y. (1991) Electroporation of cell-membranes. *Biophysical Journal*, **60** (2), 297–306.
99 Weaver, J.C. and Chizmadzhev, Y.A. (1996) Theory of electroporation: a review. *Bioelectrochemistry and Bioenergetics*, **41** (2), 135–160.
100 Teissie, J. and Tsong, T.Y. (1981) Electric-field induced transient pores in phospholipid-bilayer vesicles. *Biochemistry*, **20** (6), 1548–1554.
101 Glaser, R.W., Leikin, S.L., Chernomordik, L.V., Pastushenko, V.F., and Sokirko, A.I. (1988) Reversible electrical breakdown of lipid bilayers – formation and evolution of pores. *Biochimica et Biophysica Acta*, **940** (2), 275–287.
102 Kinosita, K.J., Hibino, M., Itoh, H., Shigemori, M., Hirano, K., Kirino, Y., and Hayakawa, T. (1992) Events of membrane elecroporation visualized on a time scale from microseconds to seconds, in *Guide to Electroporation and Electrofusion* (eds D.C. Chang, B.M. Chassy, J.A. Saunders, and A.E. Sowers), Academic Press, New York, pp. 29–46.
103 Zhelev, D.V. and Needham, D. (1993) Tension-stabilized pores in giant vesicles – determination of pore-size and pore line tension. *Biochimica et Biophysica Acta*, **1147** (1), 89–104.
104 Sandre, O., Moreaux, L., and Brochard-Wyart, F. (1999) Dynamics of transient pores in stretched vesicles. *Proceedings of the National Academy of Sciences of the USA*, **96** (19), 10591–10596.
105 Tekle, E., Astumian, R.D., Friauf, W.A., and Chock, P.B. (2001) Asymmetric pore distribution and loss of membrane lipid in electroporated DOPC vesicles. *Biophysical Journal*, **81** (2), 960–968.
106 Rodriguez, N., Cribier, S., and Pincet, F. (2006) Transition from long- to short-lived transient pores in giant vesicles in an aqueous medium. *Physical Review E*, **74** (6), 061902.
107 Riske, K.A. and Dimova, R. (2006) Electric pulses induce cylindrical deformations on giant vesicles in salt solutions. *Biophysical Journal*, **91** (5), 1778–1786.

108 Krassowska, W. and Filev, P.D. (2007) Modeling electroporation in a single cell. *Biophysical Journal*, **92** (2), 404–417.

109 Harbich, W. and Helfrich, W. (1979) Alignment and opening of giant lecithin vesicles by electric fields. *Zeitschrift fur Naturforschung A*, **34** (9), 1063–1065.

110 Portet, T. and Dimova, R. (2010) A new method for measuring edge tensions and stability of lipid bilayers: effect of membrane composition. *Biophysical Journal*, **99**, 3264–3273.

111 Knorr, R.L., Staykova, M., Gracia, R.S., and Dimova, R. (2010) Wrinkling and electroporation of giant vesicles in the gel phase. *Soft Matter*, **6** (9), 1990–1996.

112 Cerda, E. and Mahadevan, L. (2003) Geometry and physics of wrinkling. *Physical Review Letters*, **90** (7), 074302.

113 Cerda, E., Ravi-Chandar, K., and Mahadevan, L. (2002) Thin films–wrinkling of an elastic sheet under tension. *Nature*, **419** (6907), 579–580.

114 Finken, R. and Seifert, U. (2006) Wrinkling of microcapsules in shear flow. *Journal of Physics: Condensed Matter*, **18** (15), L185–L191.

115 Elmashak, E.M. and Tsong, T.Y. (1985) Ion selectivity of temperature-induced and electric-field induced pores in dipalmitoylphosphatidylcholine vesicles. *Biochemistry*, **24** (12), 2884–2888.

116 Risselada, H.J. and Marrink, S.J. (2009) The freezing process of small lipid vesicles at molecular resolution. *Soft Matter*, **5**, 4531–4541.

117 Evans, E. and Heinrich, V. (2003) Dynamic strength of fluid membranes. *Comptes Rendus Physique*, **4** (2), 265–274.

118 Boucher, P.A., Joos, B., Zuckermann, M.J., and Fournier, L. (2007) Pore formation in a lipid bilayer under a tension ramp: modeling the distribution of rupture tensions. *Biophysical Journal*, **92** (12), 4344–4355.

119 Leontiadou, H., Mark, A.E., and Marrink, S.J. (2004) Molecular dynamics simulations of hydrophilic pores in lipid bilayers. *Biophysical Journal*, **86** (4), 2156–2164.

120 Mukherjee, S. and Maxfield, F.R. (2004) Membrane domains. *Annual Review of Cell and Developmental Biology*, **20**, 839–866.

121 Gabriel, B. and Teissie, J. (1997) Direct observation in the millisecond time range of fluorescent molecule asymmetrical interaction with the electropermeabilized cell membrane. *Biophysical Journal*, **73** (5), 2630–2637.

122 Gabriel, B. and Teissie, J. (1999) Time courses of mammalian cell electropermeabilization observed by millisecond imaging of membrane property changes during the pulse. *Biophysical Journal*, **76** (4), 2158–2165.

123 Discher, B.M., Won, Y.Y., Ege, D.S., Lee, J.C.M., Bates, F.S., Discher, D.E., and Hammer, D.A. (1999) Polymersomes: tough vesicles made from diblock copolymers. *Science*, **284** (5417), 1143–1146.

124 Dimova, R., Seifert, U., Pouligny, B., Förster, S., and Döbereiner, H.-G. (2002) Hyperviscous diblock copolymer vesicles. *European Physical Journal B*, **7**, 241–250.

125 Kantsler, V., Segre, E., and Steinberg, V. (2007) Vesicle dynamics in time-dependent elongation flow: wrinkling instability. *Physical Review Letters*, **99** (17), 178102.

126 Lipowsky, R. and Dobereiner, H.G. (1998) Vesicles in contact with nanoparticles and colloids. *Europhysics Letters*, **43** (2), 219–225.

127 Sens, P. and Isambert, H. (2002) Undulation instability of lipid membranes under an electric field. *Physical Review Letters*, **88** (12), 128102.

128 Petrov, A.G. (1984) Flexoelectricity of lyotropics and biomembranes. *Nuovo Cimento della Societa Italiana di Fisica D*, **3** (1), 174–192.

129 Petrov, A.G. and Bivas, I. (1984) Elastic and flexoelectic aspects of out-of-plane fluctuations in biological and model membranes. *Progress in Surface Science*, **16** (4), 389–512.

130 Petrov, A.G. (2002) Flexoelectricity of model and living membranes. *Biochimica et Biophysica Acta*, **1561** (1), 1–25.

131 Gao, L.T., Feng, X.Q., Yin, Y.J., and Gao, H.J. (2008) An electromechanical liquid crystal model of vesicles. *Journal*

of the Mechanica and Physics of Solids, **56** (9), 2844–2862.

132 Simons, K. and Ikonen, E. (1997) Functional rafts in cell membranes. *Nature*, **387** (6633), 569–572.

133 Dietrich, C., Bagatolli, L.A., Volovyk, Z.N., Thompson, N.L., Levi, M., Jacobson, K., and Gratton, E. (2001) Lipid rafts reconstituted in model membranes. *Biophysical Journal*, **80** (3), 1417–1428.

134 Evans, E. and Rawicz, W. (2094) 1990) Entropy-driven tension and bending elasticity in condensed-fluid membranes. *Physical Review Letters*, **64** (17), 2097.

135 Song, J.B. and Waugh, R.E. (1993) Bending rigidity of SOPC membranes containing cholesterol. *Biophysical Journal*, **64** (6), 1967–1970.

136 Meleard, P., Gerbeaud, C., Pott, T., FernandezPuente, L., Bivas, I., Mitov, M.D., Dufourcq, J., and Bothorel, P. (1997) Bending elasticities of model membranes: influences of temperature and sterol content. *Biophysical Journal*, **72** (6), 2616–2629.

137 Henriksen, J., Rowat, A.C., Brief, E., Hsueh, Y.W., Thewalt, J.L., Zuckermann, M.J., and Ipsen, J.H. (2006) Universal behavior of membranes with sterols. *Biophysical Journal*, **90** (5), 1639–1649.

138 Pan, J.J., Mills, T.T., Tristram-Nagle, S., and Nagle, J.F. (2008) Cholesterol perturbs lipid bilayers nonuniversally. *Physical Review Letters*, **100** (19), 198103.

139 Pan, J., Tristram-Nagle, S., Kucerka, N., and Nagle, J.F. (2008) Temperature dependence of structure, bending rigidity, and bilayer interactions of dioleoylphosphatidylcholine bilayers. *Biophysical Journal*, **94** (1), 117–124.

140 Mathai, J.C., Tristram-Nagle, S., Nagle, J.F., and Zeidel, M.L. (2008) Structural determinants of water permeability through the lipid membrane. *Journal of General Physiology*, **131** (1), 69–76.

141 Karatekin, E., Sandre, O., Guitouni, H., Borghi, N., Puech, P.H., and Brochard-Wyart, F. (2003) Cascades of transient pores in giant vesicles: line tension and transport. *Biophysical Journal*, **84** (3), 1734–1749.

142 Riske, K.A., Knorr, R.L., and Dimova, R. (2009) Bursting of charged multicomponent vesicles subjected to electric pulses. *Soft Matter*, **5**, 1983–1986.

143 Raffy, S. and Teissie, J. (1999) Control of lipid membrane stability by cholesterol content. *Biophysical Journal*, **76** (4), 2072–2080.

144 Genco, I., Gliozzi, A., Relini, A., Robello, M., and Scalas, E. (1993) Electroporation in symmetrical and asymmetric membranes. *Biochimica et Biophysica Acta*, **1149** (1), 10–18.

145 Isambert, H. (1998) Understanding the electroporation of cells and artificial bilayer membranes. *Physical Review Letters*, **80** (15), 3404–3407.

146 Betterton, M.D. and Brenner, M.P. (1999) Electrostatic edge instability of lipid membranes. *Physical Review Letters*, **82** (7), 1598–1601.

147 Kumaran, V. (2000) Instabilities due to charge-density-curvature coupling in charged membranes. *Physical Review Letters*, **85** (23), 4996–4999.

148 Schwister, K. and Deuticke, B. (1985) Formation and properties of aqueous leaks induced in human erythrocytes by electrical breakdown. *Biochimica et Biophysica Acta*, **816** (2), 332–348.

149 Kinosita, K. and Tsong, T.Y. (1977) Formation and resealing of pores of controlled sizes in human erythrocyte membrane. *Nature*, **268** (5619), 438–441.

150 Tekle, E., Astumian, R.D., and Chock, P.B. (1994) Selective and asymmetric molecular-transport across electroporated cell membranes. *Proceedings of the National Academy of Sciences of the USA*, **91** (24), 11512–11516.

151 Litster, J.D. (1975) Stability of lipid bilayers and red blood-cell membranes. *Physics Letters A*, **53** (3), 193–194.

152 Newman, C.M.H. and Bettinger, T. (2007) Gene therapy progress and prospects: ultrasound for gene transfer. *Gene Therapy*, **14** (6), 465–475.

153 Escoffre, J.M., Portet, T., Wasungu, L., Teissie, J., Dean, D., and Rols, M.P. (2009) What is (still not) known of the mechanism by which electroporation

mediates gene transfer and expression in cells and tissues. *Molecular Biotechnology*, **41** (3), 286–295.

154 Chang, D.C. and Reese, T.S. (1990) Changes in membrane structure induced by electroporation as revealed by rapid-freezing electron microscopy. *Biophysical Journal*, **58** (1), 1–12.

155 Chang, D.C. (1992) Structure and dynamics of electric field-induced membrane pores as revealed by rapid-freezing electron microscopy, in *Guide to Electroporation and Electrofusion* (eds D.C. Chang, B.M. Chassy, J.A. Saunders, and A.E. Sowers), Academic Press, San Diego, pp. 9–27.

156 Puech, P.H., Borghi, N., Karatekin, E., and Brochard-Wyart, F. (2003) Line thermodynamics: adsorption at a membrane edge. *Physical Review Letters*, **90** (12), 128304.

157 Srividya, N. and Muralidharan, S. (2008) Determination of the line tension of giant vesicles from pore-closing dynamics. *Journal of Physical Chemistry B*, **112** (24), 7147–7152.

158 Portet, T., Dimova, R., Dean, D.S., and Rols, M.-P. (2010) Electric fields and giant vesicles. *Biophysical Journal*, **98** (3 Suppl. 1), 77a.

159 Ellens, H., Bentz, J., and Szoka, F.C. (1986) Fusion of phosphatidylethanolamine-containing liposomes and mechanism of the L_{α}-H_{II} phase-transition. *Biochemistry*, **25** (14), 4141–4147.

160 Lewis, R.N.A.H. and McElhaney, R.N. (1993) Calorimetric and spectroscopic studies of the polymorphic phase behavior of a homologous series of n-saturated 1,2-diacyl phosphatidylethanolamines. *Biophysical Journal*, **64** (4), 1081–1096.

161 Pink, D.A., McNeil, S., Quinn, B., and Zuckermann, M.J. (1998) A model of hydrogen bond formation in phosphatidylethanolamine bilayers. *Biochimica et Biophysica Acta*, **1368** (2), 289–305.

162 Kinosita, K. and Tsong, T.Y. (1977) Voltage-induced pore formation and hemolysis of human erythrocytes. *Biochimica et Biophysica Acta*, **471** (2), 227–242.

163 Chang, D.C., Chassy, B.M., Saunders, J.A., and Sowers, A.E. (eds) (1992) *Guide to Electroporation and Electrofusion*, Academic Press, San Diego.

164 Zimmermann, U. and Neil, G.A. (eds) (1996) *Electromanipulation of Cells*, CRC Press, Boca Raton.

165 Zimmermann, U. (1986) Electrical breakdown, electropermeabilization and electrofusion. *Reviews of Physiology Biochemistry and Pharmacology*, **105**, 175–256.

166 Llinas, R., Steinberg, I.Z., and Walton, K. (1981) Relationship between presynaptic calcium current and postsynaptic potential in squid giant synapse. *Biophysical Journal*, **33** (3), 323–351.

167 Lindau, M. and de Toledo, G.A. (2003) The fusion pore. *Biochimica et Biophysica Acta*, **1641** (2–3), 167–173.

168 Hafez, I., Kisler, K., Berberian, K., Dernick, G., Valero, V., Yong, M.G., Craighead, H.G., and Lindau, M. (2005) Electrochemical imaging of fusion pore openings by electrochemical detector arrays. *Proceedings of the National Academy of Sciences of the USA*, **102** (39), 13879–13884.

169 Shillcock, J.C. and Lipowsky, R. (2005) Tension-induced fusion of bilayer membranes and vesicles. *Nature Materials*, **4** (3), 225–228.

170 Veatch, S.L. and Keller, S.L. (2003) Separation of liquid phases in giant vesicles of ternary mixtures of phospholipids and cholesterol. *Biophysical Journal*, **85** (5), 3074–3083.

171 Kahya, N., Scherfeld, D., Bacia, K., Poolman, B., and Schwille, P. (2003) Probing lipid mobility of raft-exhibiting model membranes by fluorescence correlation spectroscopy. *Journal of Biological Chemistry*, **278** (30), 28109–28115.

172 Chiu, D.T., Wilson, C.F., Ryttsen, F., Stromberg, A., Farre, C., Karlsson, A., Nordholm, S., Gaggar, A., Modi, B.P., Moscho, A., Garza-Lopez, R.A., Orwar, O., and Zare, R.N. (1999) Chemical transformations in individual ultrasmall biomimetic containers. *Science*, **283** (5409), 1892–1895.

173 Fischer, A., Franco, A., and Oberholzer, T. (2002) Giant vesicles as microreactors

for enzymatic mRNA synthesis. *ChemBioChem*, **3** (5), 409–417.
174 Kulin, S., Kishore, R., Helmerson, K., and Locascio, L. (2003) Optical manipulation and fusion of liposomes as microreactors. *Langmuir*, **19** (20), 8206–8210.
175 Noireaux, V. and Libchaber, A. (2004) A vesicle bioreactor as a step toward an artificial cell assembly. *Proceedings of the National Academy of Sciences of the USA*, **101** (51), 17669–17674.
176 Yang, P., Lipowsky, R., and Dimova, R. (2009) Nanoparticle formation in giant vesicles: synthesis in biomimetic compartments. *Small*, **5** (18), 2033–2037.
177 Cohen, F.S., Akabas, M.H., and Finkelstein, A. (1982) Osmotic swelling of phospholipid-vesicles causes them to fuse with a planar phospholipid-bilayer membrane. *Science*, **217** (4558), 458–460.
178 Grafmuller, A., Shillcock, J., and Lipowsky, R. (2007) Pathway of membrane fusion with two tension-dependent energy barriers. *Physical Review Letters*, **98** (21), 218101.
179 Estes, D.J., Lopez, S.R., Fuller, A.O., and Mayer, M. (2006) Triggering and visualizing the aggregation and fusion of lipid membranes in microfluidic chambers. *Biophysical Journal*, **91** (1), 233–243.
180 Lentz, B.R. (2007) PEG as a tool to gain insight into membrane fusion. *European Biophysical Journal*, **36** (4–5), 315–326.
181 Kunishima, M., Tokaji, M., Matsuoka, K., Nishida, J., Kanamori, M., Hioki, K., and Tani, S. (2006) Spontaneous membrane fusion induced by chemical formation of ceramides in a lipid bilayer. *Journal of the American Chemical Society*, **128** (45), 14452–14453.
182 Jahn, R., Lang, T., and Sudhof, T.C. (2003) Membrane fusion. *Cell*, **112** (4), 519–533.
183 Bhattacharya, D. and Gupta, R.K. (2005) Nanotechnology and potential of microorganisms. *Critical Reviews in Biotechnology*, **25** (4), 199–204.
184 Mandal, D., Bolander, M.E., Mukhopadhyay, D., Sarkar, G., and Mukherjee, P. (2006) The use of microorganisms for the formation of metal nanoparticles and their application. *Applied Microbiology and Biotechnology*, **69** (5), 485–492.
185 Sanchez, C., Arribart, H., and Guille, M.M.G. (2005) Biomimetism and bioinspiration as tools for the design of innovative materials and systems. *Nature Materials*, **4** (4), 277–288.
186 Dickerson, M.B., Sandhage, K.H., and Naik, R.R. (2008) Protein- and peptide-directed syntheses of inorganic materials. *Chemical Reviews*, **108** (11), 4935–4978.
187 Mann, S., Hannington, J.P., and Williams, R.J.P. (1986) Phospholipid-vesicles as a model system for biomineralization. *Nature*, **324** (6097), 565–567.
188 Bhandarkar, S. and Bose, A. (1990) Synthesis of nanocomposite particles by intravesicular coprecipitation. *Journal of Colloid and Interface Science*, **139** (2), 541–550.
189 Khramov, M.I. and Parmon, V.N. (1993) Synthesis of ultrafine particles of transition-metal sulfides in the cavities of lipid vesicles and the light-stimulated transmembrane electron-transfer catalyzed by these particles. *Journal of Photochemistry and Photobiology A*, **71** (3), 279–284.
190 Korgel, B.A. and Monbouquette, H.G. (2000) Controlled synthesis of mixed core and layered (Zn,Cd)S and (Hg,Cd)S nanocrystals within phosphatidylcholine vesicles. *Langmuir*, **16** (8), 3588–3594.
191 Ishikawa, K., Sato, K., Shima, Y., Urabe, I., and Yomo, T. (2004) Expression of a cascading genetic network within liposomes. *FEBS Letters*, **576** (3), 387–390.
192 Kita, H., Matsuura, T., Sunami, T., Hosoda, K., Ichihashi, N., Tsukada, K., Urabe, I., and Yomo, T. (2008) Replication of genetic information with self-encoded replicase in liposomes. *ChemBioChem*, **9** (15), 2403–2410.
193 Hsin, T.M. and Yeung, E.S. (2007) Single-molecule reactions in liposomes. *Angeweldte Chemie International Edition*, **46** (42), 8032–8035.
194 Christensen, S.M. and Stamou, D. (2007) Surface-based lipid vesicle reactor systems: fabrication and applications. *Soft Matter*, **3** (7), 828–836.

Keywords/Abstract

Dear Author,

Keywords and abstracts will not be included in the print version of your chapter but only in the online version.

Please check and/or supply keywords. If you supplied an abstract with the manuscript, please check the typeset version.

If you did not provide an abstract, the section headings will be displayed instead of an abstract text in the online version.

Keywords
membrane electroporation, electrodeformation, electrofusion, gene transfer, drug transfer, giant unilamellar vesicles, electric fields

Abstract
Achieving control of biomedical applications like electrochemotherapy and gene or drug transfer mediated by electric fields requires understanding of the mechanisms behind electroporation in cells. Bottom-up approaches in this direction are based on collecting knowledge at the level of simple biomimetic systems like model membranes. In this chapter, attention is focused on the response to electric fields and electroporation of such model membranes exemplified by giant unilamellar vesicles. Being a model system with cell-size dimensions, giant vesicles provide us with a convenient tool to directly visualize under the microscope the response of lipid bilayers to electric fields. The chapter summarizes various types of behavior observed when vesicles are exposed to strong direct current pulses. Different processes such as electrodeformation, electroporation, and electrofusion of giant vesicles are considered. The dynamics of the vesicle response with a resolution below milliseconds for all of these processes are described and discussed in terms of the characteristic material properties of the membranes. New aspects of the behavior of vesicles made of membranes containing cholesterol or charged lipids, in the fluid or in the gel phase, and embedded in different solutions, are introduced. The membrane stability and lifetime of pores induced by electric pulses are discussed in terms of critical poration potentials and membrane edge tension. Beyond the area of biomedical applications, the chapter considers some application aspects of vesicle electrofusion for creating multidomain membranes and establishing nanoparticle synthesis in vesicles as microreactors.